University of Amsterdam

SFES: Master Thesis

Quantum dots for electron-beam lithography

Author:
Weiyi Ding

Supervisor:
Dr. Bruno Ehrler

Daily Supervisor:
Christian Dieleman

December 16, 2020

Universiteit van Amsterdam

Abstract

Within nanoscience, quantum dots (QDs) have gained interest due to their tunable, precise optoelectronic and optical properties. They are emerging materials for research in nanophotonics and nanotechnology. Whereas the valence and conduction band of a semiconductor bulk material are continuous, QDs have discrete energy states for the electrons, leading to narrow peaks in the absorption and emission spectra. Moreover, the bandgap depends on the size and shape of the QD, these are tunable during synthesis. These two main benefits make QDs a promising material for nanofabrication.

A well-known technique for fabricating nanostructures is electron-beam (e-beam) lithography. The e-beam resist is patterned by incoming electrons, which alter the molecular structure with their kinetic energy and charge and thereby change the solubility in the exposed areas. This direct lithography has the simplification that no mask is needed, in contrast with conventional lithography where masks and intermediate layers are used for material deposition or etching.

In this project two types of QDs, cadmium selenide (CdSe) and lead sulfide (PbS), are investigated as e-beam resist for direct exposure. The practical resolution limit of e-beam and the limiting factors are hard to define. They depend on the lithography equipment and the e-beam resist. Here, the aim is to pattern QD nanostructures and subsequently measure and analyse changes in the structures to gain understanding the interaction between electrons and QDs. The experimental resolution limit is found to be 20 nm, and only a very small fraction of the electrons cause the solubility change in QDs. Contributing factors of the patterning resolution are adhesion between QDs and the silicon (Si) substrate, thickness of the QD layers, and type of development solution. Results show that the QDs photoluminescence is maintained after exposure, indicating a possible mechanism during the exposure; cross-linking between the ligands of QDs.

Contents

1 Introduction

Since the emergence of electronics, exceeding the limit of miniaturization in mechanical, optical and electronic systems has been the drive for development and research. New techniques are constantly pushing the resolution limit of features, known as the smallest feature that can be printed with acceptable quality for a desired purpose, further down into single nanometer range to meet the continuing challenge of smaller component size in the system[1]. Component sizes used to be in tens of micrometers became single digit micrometers, then hundreds of nanometers, and nowadays they are approaching tens and even a few nanometers[2]. The main driver for developments in nanotechnology has been the industrial interest in integrated circuits, this is constantly being pushed further down into the single nanometer range by researchers' efforts to overcome the various limitations of resolution. Also fundamental research fields of nanophotonics and photovoltaics encourage the search for adequate complex materials and high resolution lithography technologies on nanoscale. This research requires to understand the complex fundamental mechanisms behind matter, light, electrons, and their interactions[3].

As the resolution keeps on increasing, techniques of lithography are constantly facing the challenge of developing smaller features and discovering new resist materials that fit the requirements. In other words, realizing a higher resolution nanoscale lithography asks for high quality nanofabrication systems and innovative nanomaterials as resist for its lithography purpose. This is very challenging because of the precision needed to make extremely fine patterns that approaches tens of nanometres nowadays[4]. These patterned nanostructures are critical for the integration with solid-state devices. Very few materials are suitable for such a small nanoscale fabrication. Also, some other requirements are attached to material choice such as safety, efficient production, and accurate electrical properties[5].

One interesting type of nanoparticles that has gained attention over the past decades in nanomaterial science are quantum dots (QDs). They are made of semiconductor particles surrounded by organic molecules, only a few nanometres in size. Their optoelectronic properties depend on their size and shape. Different sizes and structure designs from the same material can provide diverse electronic functionalities, making them extremely beneficial for nanofabrication in optoelectronic devices such as light emitting diode(LED), photodetectors, field-effect transistors, photovoltaic cells, and photodetectors[6].

1.1 QDs as emitters

QDs are considered good emitters because of their beneficial optoelectronic properties. They show relatively high luminescence performances which can be adjusted to the desired range by changing their size or shape, making them unique compared to other luminescent materials[1]. The explanation is at the core of nanophotonics and quantum optics. As

a nanoparticle becomes smaller and in its size, quantum physical effects appear. In this nanoscale limit, the absorption and emission characteristics of the particle become different than those of the bulk composition, even though the particles are the same[7]. The underlying theory will be given in more detail in Chapter 2.

The high luminescence efficiency and bright colours of QDs highlight their potential in luminescent energy-efficient, high-colour-quality applications. Some are already on the market such as LED thin-film displays, and solid-state lighting (*SSL*) applications[8]. QDs are capable of presenting more accurate and outstanding colours, showing brighter emission performances in the region of the human visible spectrum, even near infrared(*IR*). QDs with luminescence near IR, in the range of 780 - 2500 nm, have the potential for use in night-vision- displays and face identification systems[8]. Figure 1 shows the difference in optical range of QDs for LED display and SSL applications, using a CIE chromaticity diagram.

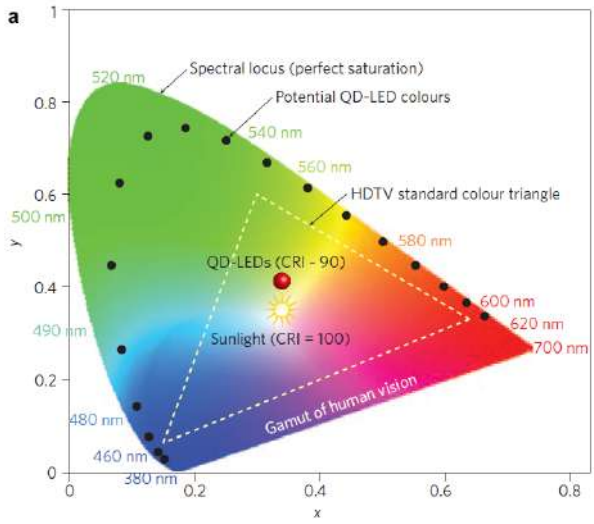

Figure 1: *CIE chromaticity diagram, showing that the spectral purity of QDs enables a colour gamut, indicated by the dotted line, larger than the high-definition television (HDTV) standard, indicated by dashed line. Figure is adopted from [8]*

Another promising QD application is in the medical area, for bio-imaging. Compared to the present particles in bio-imaging, QDs have a higher quantum yield, which means they are much brighter, and they show higher photostabilily. Furthermore, the fluorescent probes in bio-imaging have to remain well-dispersed and stable in aqueous medium with a wide range of pH and ionic strengths [9][10]. Many approaches have been developed to make the QDs water-dispersible, which is a neccesary property for being applicable for diagnosis of diseases, the study of embryogenesis, and lymphocyte immunology [9] [10]. An example QD bio-image is shown in figure 2, QD show a higher photostability compared to the other dye (*Alexa 488*).

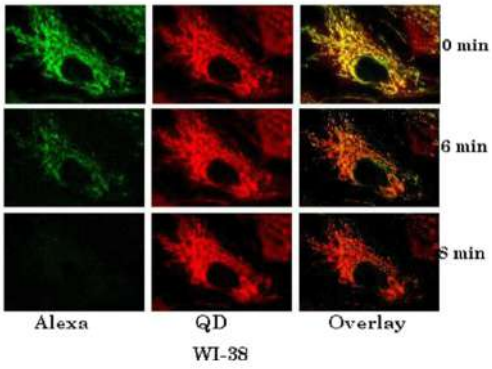

Figure 2: *Immunofluorescence images of human mitochondrial(mortalin) made with Alexa 488 and QD, comparing the photostability in normal cells[11], vertical axes indicates three different times.*

Besides industrial purposes, QDs are very attractive for nanophotonic and photovoltaic research fields because of the aforementioned properties. QDs can be seen as auspicious materials for fabricating complex functional nanostructures in order to study and manage the behaviour of light and electrons. By altering the structure, the exposed regions can undergo further various chemical transformations, as they become partially sealed off from the external environment. The group of Palazon have shown that TOPO-capped CdSe/CdS QD films can be transformed to Cu_2Se/Cu_2S by cation-exchange reactions with copper precursors[12]. Prior to this exchange, the precursors were dissolved in solvents in which the QDs were not dispersible, otherwise the QDs would be damaged. After exposure to e-beam, they became sensitive to cation exchange. Hence when the whole film after irradiation is exposed to a solution containing copper metal-ion species, it develops into a patterned film of cadmium and copper chalcogenide QDs, shown in Figure 3. This approach was used to define luminescent patterns of cadmium chalcogenides on a layer of non-luminescent copper chalcogenides[12].

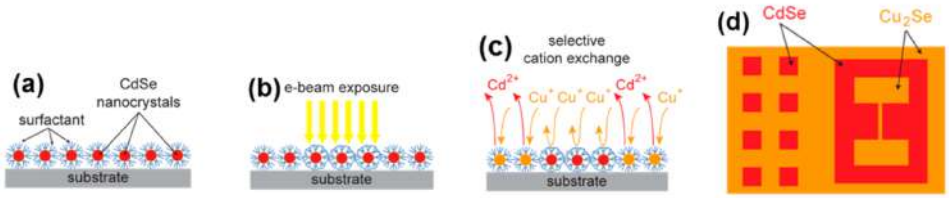

Figure 3: *Selective cation exchange, PL and chemical maps of CsPbBr3/CsPbI3 films by X-ray lithography. Figure adopted from [12]*

Moreover, they have shown that this process be applied to tune the specific chemical composition, subsequently the properties of irradiated and non-irradiated QDs, which al-

lows for more complex patterning of QD films. As it allows the modification of the QDs themselves, it opens a new set of possible applications in thin film nanofabrication that was until now impossible to obtain.

1.2 E-beam lithography

Nanostructures are fabricated through lithography, a crucial step in the manufacturing process of the semiconductor industry. Precise patterns on the nanoscale are formed on the wafer in order to transfer the image from a mask to a radiation-sensitive chemical mixture called a resist, often comprised of several components[13]. Lithography systems in the industry are photolithography systems (also called optical lithography), where masks are applied to make interference patterns. A light source passes through a mask with transparent and opaque regions, projecting patterns to the substrate[14]. This main technology used today is predicted to be applicable at 45 nm of feature sizes in the integrated circuits, with the use 13 nm wavelength Extreme Ultraviolet tools[5]. But interference patterns cannot exceed the diffraction limit and it is not applicable for unique, complex patterns. This is where e-beam lithography has more to offer, it uses electrons instead of photons. Electrons have much smaller wavelengths, they beat the optical diffraction limit and make features in the smaller nanoscale regime. E-beam lithography can produce pattern line widths on the order of 10 nm, also unique complex designs for which a photomask is hard to create[2]. The finest structures are achieved by scanning a focused beam of electrons, containing an extremely small dose energy electrons, to draw designed shapes on a surface covered with an electron-sensitive resist[14], the process is schematically shown in figure 4. Despite these benefits, e-beam lithography is rather applicable for smaller-scale fundamental research or prototyping [14] and not for industry. It is more expensive than photolithography and requires clean room facilities.

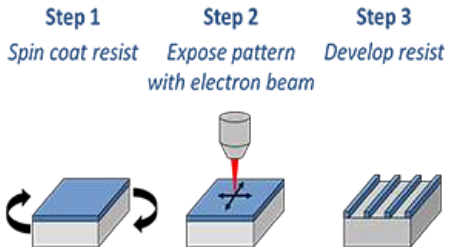

Figure 4: *Schematically e-beam lithography process, figure adopted from [15]*

Conventional e-beam lithography uses multiple layers of e-beam resist with different electron sensitivities and multiple exposure steps. One e-beam induces one layer to adjust the molecular structure and thus the physical property. A change in solubility occurs in the part that is either exposed or non-exposed[3]. Since multiple steps involve intermediate depositions, developments or lift-offs, and etchings[13], technical complications are more

likely to occur and it is more time consuming compared to direct patterning, a methodology that only requires one type of resist and the exposure is performed directly on the material of interest.

1.3 The Project: CdSe and PbS for e-beam lithography

In this project, QDs are applied as resist for direct e-beam lithography, which is a relative new combination. So far, conventional e-beam resists such as *Nippon Zeon (ZEP 520)*, *hydrogen silsesquioxane(HSQ)* and *polymethylmetacrylaat (PMMA)* are generally used due to their high sensitivity, stability, scalability and precision[2]. However, more steps are needed to make nanostructures. Here, a strategy of direct patterning and contributing factors are reported for QDs as resist. Direct patterning offers a significant simplification in processing by using the functional component as the only resist on the substrate, this is a negative resist [14]. Direct patterning avoids the complications of resist deposition, etching and removal, thus avoiding issues of film adhesion, long processing times and roughness generation during the etching step. It offers a simple and yet highly accurate approach towards the nanostructures resolution limit.

This project investigates QDs as e-beam resist for direct patterning. So far, only few reports have shown this application. According to the latest developments on this topic, the electron energy alters the QD structure during exposure[6][12], and they preserve the properties after exposure. As an extension of this promising technique, we focus on direct patterning of two QD types; PbS and CdSe. Both are synthesized according known hot-injection methods. The overall aim is to pattern QDs as small as possible on substrates, investigate the contributing factors to the optimal resolution, and gain information about the exposure mechanisms.

The thesis is structured as follows. First, theoretical background on QDs and e-beam lithography is given in Chapter 2. Starting with the underlying fundamental physics of QDs, as an emerging nanomaterial for emitting purposes in devices. Then, the basic working mechanism of e-beam lithography is explained in 2.2 and 2.3. Chapter 2 ends with a summary of previous work. Chapter 3 describes the used experimental methods and measurements. Followed by data processing and analyses in Chapter 4, including discussion. Chapter 5 finishes with a summary and core conclusion. Eventually, potential future outcomes of this still incipient technique will be discussed, pinpointing the major bottlenecks for a widespread use of this approach in nanofabrication and suggesting different means to overcome them.

2 Theoretical background

This chapter provides the required theoretical foreknowledge about QDs and e-beam lithography, to understand their properties in the context and purpose of this research. First, fundamentals of QDs will be explained more in detail, their special physical properties are highlighted and the composition of the applied QDs for this specific synthesis is elaborated. Subsequently the characterization, the technology behind e-beam lithography, the distribution and energy deposition of electrons will be explained. Leading to the combination of e-beam and QDs, a new possibility of using QDs as resist. But also the remaining open questions about interactions between e-beam and QDs. Such as how electrons are distributed into the resist, how the energy is deposited on the molecular level, and how QDs are altered in their structure after exposure, the latter is central to this research.

2.1 Quantum Dots

In solid-state physics, the electronic band structure describes the range of allowed energy levels of an electron within a given solid structure. For semiconductors, an energy level that is not allowed for an electron is called a bandgap[16]. Semiconductor bulk materials have a bandgap between valence and conduction band, which indicates to the difference between the maximum of the valence band and the minimum of the conduction band, in momentum space of electrons. It is the required energy to promote a valence electron that is bounded to an atom, to become a conduction electron. This conduction electron is then free to move within the lattice structure and serve as a charge carrier to conduct electric current [17]. The required energy can be provided by a photon or an incoming electron.

2.1.1 Quantum confinement

The interaction between photons and QDs can be explained from nanophotonics. With the decreasing size of the nanoparticles, quantum physical effects become apparent when photons get absorbed by these particles[18, 19]. Continuous absorption and the continuous luminescence are replaced by discrete resonant interactions. Some particles that belong to these so-called confined systems are fluorescent atoms, molecules, semiconductor nanoparticles. The resonances are found at optical eigenfrequencies of the particles [16].

QDs are semiconductor nanoparticles, whose band structures are different from semiconductor bulk materials structures. The first nanoparticle experiments were executed in 1980s, with colloidal dispersion of semiconductor nanocrystals and these experiments were directed at energy conversion applications [20, 19]. One major discovery was that colloidal dispersion solutions of the same semiconductor type showed different fluorescence colors. The only difference between them was the nanocrystals size, which was the result of different growth duration during synthesis [21, 19]. This difference in fluorescence color is attributed

to the quantum confinement effect [19]. Due to the small size of QDs, their shape is often considered zero-dimensional in electron wave function determination[22].

The allowed energy levels for electrons become more discrete along with the smaller size of the particles, rather than being continuous as in the bulk material. These individual energy levels separate in energy space, leading to a reduction of the average density of states per energy range [22]. In other words, the number of states per energy range goes down, this is called level discretization. The discrete energy levels in the valence and conduction bands lead to the characteristics that make QDs so special. After absorbing a photon with a higher energy than the bandgap, an electron gets excited from the valence band into the conduction band. Together with its hole that is left behind in the valence band, they form a fixed bound state in the discrete energy levels by the electrostatic Coulomb force. This electron-hole pair is called an exciton in a quantum confinement effect[16]. One remarkable aspect is that QDs are nanometre-scale crystallites that have been reduced below the actual size of the exciton, which is called the Bohr radius[20]. Semiconductors generally contain very small effective masses of the electrons and holes. Typically, the Bohr radius of semiconductors is around 10 nm[20, 18, 19].

The confinement in QDs in three dimensions can be approximated by a spherical particle in a box. This confinement leads to quantum-size effects, with a splitting of energy levels into a series of discrete electronic transitions - in contrast to bulk materials, that have continuous energy bands. The energy range in both valence and conduction bands are shown in figure 5.

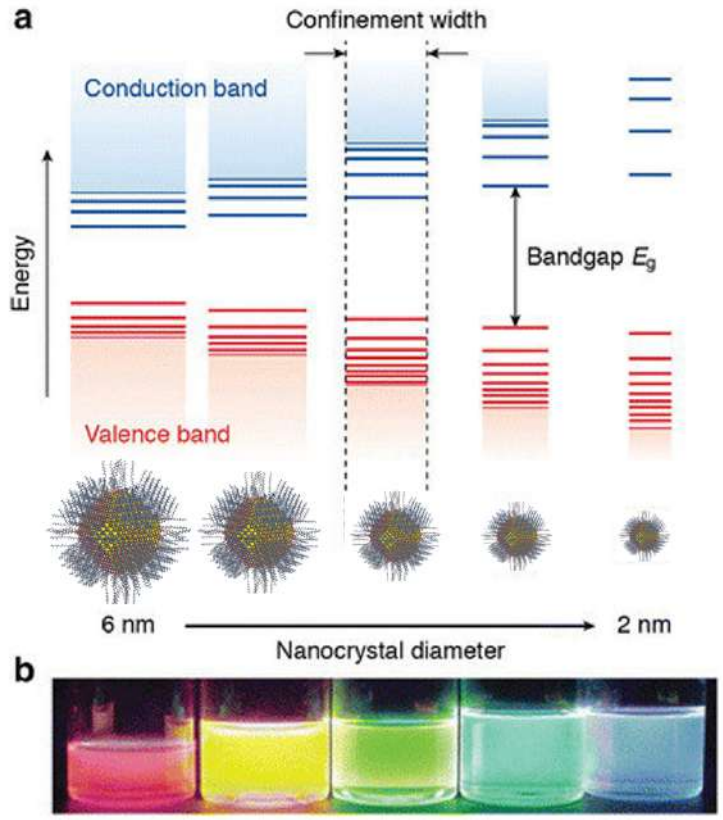

Figure 5: *QDs of decreasing sizes with matching band structure and fluorescent colour, modified figure from reference[23, 16]*

The confinement energy is described by the Heisenberg uncertainty principle, which states that the uncertainty of a particle's momentum increases if its position becomes well defined[16], and vice versa. In larger particles the Coulomb interaction between electron and hole plays a more significant role, namely, it reduces the exciton energy. Therefore the Coulomb interaction has to be taken into account[19]. But in smaller particles, the strongly shielded Coulomb interaction between electron and hole can be neglected. Smaller particles can be described by the particle-in-the-box model, the allowed energy levels move discretely upwards in the *k-space* as the box becomes smaller[18, 19]. In other words, the emission spectrum shows a blue shift as the QD is made smaller, larger QDs emit longer wavelengths resulting in emission the color red, as visible in figure 6. The specific colors and sizes vary, depending on the composition and shape of the QD[16]. Optically, QDs behave similarly to atoms, strongly absorbing specific wavelengths of the electromagnetic spectrum, while weakly absorbing the rest. One can state that QDs show intermediate behaviour between bulk semiconductors with bigger energy bands and discrete atoms or molecules[21]. The wavelength region where the QDs absorb the strongest is referred to as first absorption peak. For smaller wavelengths the QDs take on a continuously increasing absorption, indicating

that the QDs recover the bulk properties of the semiconductor. By tuning the size, one can adjust the position of the first absorption peak of the QD[16]. After absorbing photons, radiative decays occur and photons are emitted, shown in a emission spectrum, see figure 6. The ratio between the absorption and emission energy is called quantum efficiency, this is fairly high for confined excitons because energy is hardly lost by the confined electron and hole, both are well localized in a nanometer sized box inside the QD[19].

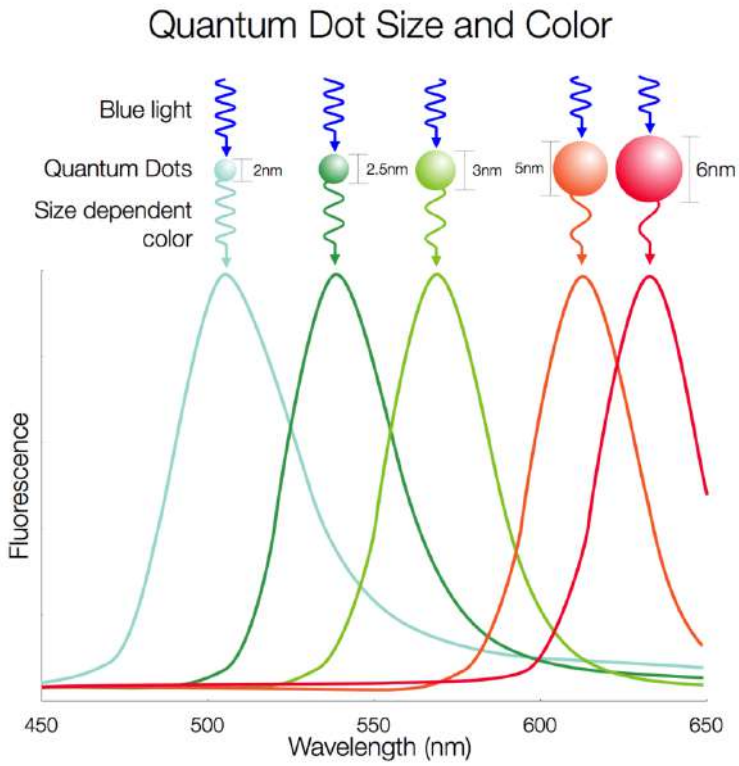

Figure 6: *Schematic emission spectrum of CdSe QD, figure adopted from [24]*

Summarized, the main beneficial properties of QDs are tunable bandgap, narrow fluorescence emission, broad absorption profiles, high color brightness, high photo- and chemical stability, and they are solution processable [25]. Therefore, it allows customization and optimization of these properties to match the application. Rendering the quality of QDs for optoelectronic components requiring both precise and variable luminescence properties, for such as transistors, solar cells, LEDs, diode and lasers [16]. Properties of QDs are determined by the type of material, structure, and synthesis circumstances. This is elaborated in the next section.

2.2 Surface passivation - QD ligands

Based on the structure and composition, QDs can be classified into different types. QDs are generally constructed from elements of Group II (Zn, Cd), -VI (Se, S), III–V, and

IV–VI of the periodic table[14]. There are various methods to synthesize of QDs, which can broadly be classified into top-down and bottom-up. The top-down approach generally refers to the breakdown of larger carbonaceous moieties, such as carbon nanotubes and graphite, also with III-V semiconductors. The bottom-up method resembles carbonization along with a means employed to block nanoparticle aggregation at high temperatures. The most common type of QDs are colloidal QDs. Colloidal QDs are synthesized from solutions, the QD product neither precipitates as bulk solid nor remains dissolved [7]. Heating the solution with the dissolved precursor at high temperature leads to decomposition of the precursor and formation of monomers. Then, they nucleate with semiconductor atoms and generate nanocrystals, the QDs. The most important parameter is temperature, it determines the optimal conditions for the QD growth. A minimum temperature must be exceeded in order to allow rearrangement and annealing of QD atoms during the synthesis process, while staying below a maximum temperature to promote QD growth and keep the particles intact[25].

The number of surface atoms of spherical shaped QDs is comparable to the number of atoms in bulk material, properties of the surface atoms can significantly affect the electronic structure of QDs[26, 19]. Chemical reactions or surface reconstruction can cause small surface defects. For 'bare' QDs, even the smallest surface defects are detrimental to the high luminescence quantum yield, since any surface defect will lead to more allowed electronic states in the bandgap region[19]. These so-called trap states will enable more non-radiative relaxation pathways, which become ascendant compared to the radiative relaxations. Consequently, the quantum yield for visible light emission decreases, making the QDs less efficient as emitters[26, 19]. Therefore, avoiding surface defects has a high priority in QD synthesis. In order to avoid the defects, QDs are typically capped with a protective layer that ideally grows epitaxially over the core, such that the chemical composition changes abruptly within one atomic layer[19]. With this protective layer, it is possible to functionalize the nanoparticles by applying surface chemistry without affecting the optical properties of the QD core itself[25, 19]. The structure of a typical QD is shown in figure7, Here, the protective layer is an amphiphilic surface, consisting of both hydrophilic and lipophilic molecules.

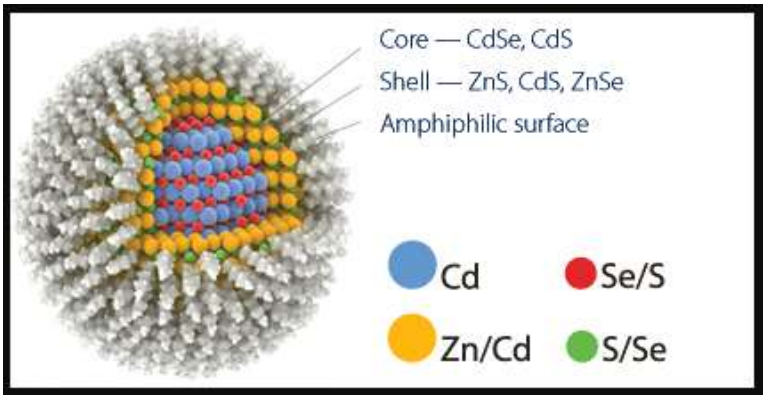

Figure 7: *Schematic chemical composition of a typical QD, figure adopted from [27].*

To function as good emitters, the absorption and emission mechanisms should be very efficient, the energy loss is as low as possible. Besides defect states, another limiting factor is the inefficient charge extraction from the active layer of the device to the electrodes. Charges have to hop from dot to dot in order to be collected. Therefore, colloidal QDs are capped by stabilising ligands, often by long insulating carbon chains and an anchoring headgroup such as oleic acid to keep them dispersed in solution during synthesis and avoid aggregation. By changing the chemical environment around the QDs after deposition, the transport can be enhanced [23]. For example by replacing the long insulating ligands to shorter ligands that can function as a binding agent, the electronic coupling between QDs will be enlarged. Nevertheless, a trade-off between the layer thickness and absorption is still present. To facilitate energy efficient carrier transport the QD-layer must be thin, however this will limit the optical path length inside the absorbing material [28].

QDs have a large surface-to-volume ratio, meaning that there is a lot of surface(mainly determined by ligand landscape) per QD in volume[7]. This ratio leads to the fact that the surfaces play a dominant role in many physical and chemical processes. On these surfaces of QD cores, ligand molecules are indispensable components of the synthesis, processing and application. As mentioned before, surface ligands enable colloidal stability and control the aggregation of QDs[7]. When the QDs come into contact with to a suitable solvent for a certain type of surface ligands, QDs disperse in the solvent. Two fundamentally different mechanisms of colloidal stabilization, steric and electrostatic, provide mostly complementary approaches to stabilize QD dispersions in several types of solvents. For instance in hydrophobic or hydrophillic liquids, by altering the chemical properties, such as changing polarity, flocculation of QDs can be induced[25]. Another stabilizing factor comes from steric hindrance, which is delaying reactions due to steric bulk composition[12]. When QDs that are passivated with organic ligands are brought into contact with a solvent, steric hindrance between the passivating layers will lead to a repulsive force between the QDs. In absence of these ligands, QDs tend to aggregate to minimize their free surface and subsequently cluster

into larger chunks that become indispersible[12, 29]. In the case of depositing QDs on a substrate, they form a film layer. Ligands are retained at the above surface, individual QDs then can be redispersed in solution[12].

Surface ligands often contain an anchoring head group and an end-functionality, both are essential components for QDs synthesis, processing and applications. The binding behaviour and functional tail of ligands can tune the dispersibility in solution and the inherent size-dependent emission[25]. Ligands can play as efficient moderators for the exciton relaxation by affecting the phonon-assisted intraband relaxation, Auger recombination or energy transfer to ligand vibrations. The photoluminescence quantum yield (PLQY) of QDs is mainly determined by the dominating radiative recombination of either band-edge excitons with the electron, or the hole-trapping processes. The use of alkylamines for example, which contain a σ-bond, usually can enhance the PLQY of CdSe QDs up to 50% due to the effective passivation for electron traps. This results in weakened non-radiative recombination of excitons[25, 26]. Some ligands are both σ - and π -donating, which can effectively passivate electron traps but introduce hole traps. Their increased or decreased effect on PLQY of QDs is therefore complicated, relying on the initial state of QD surface, the adsorption number of ligand per QD as well as the position of valence band edge of QD. The surface ligands must be careful screened to control the fluorescence emissions.

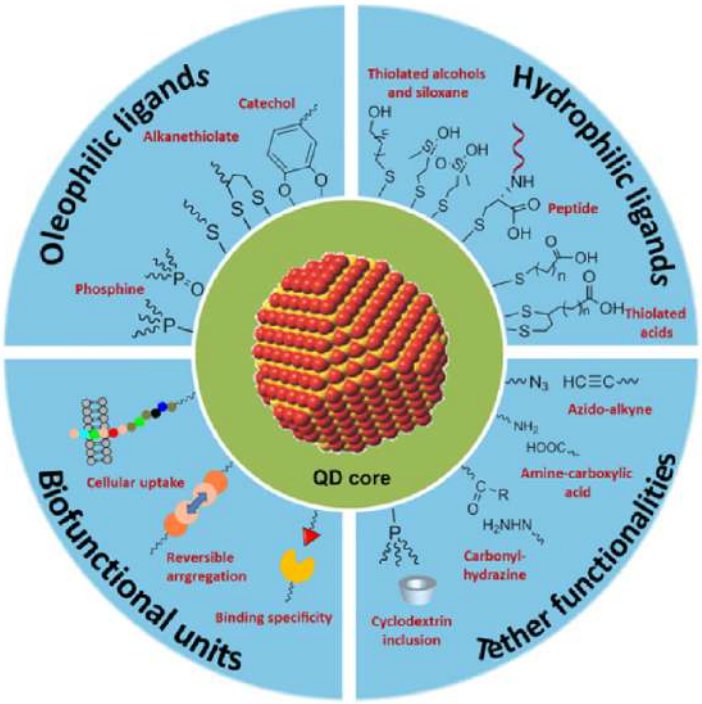

Figure 8: *Surface engineering strategies of QDs for applications. Devided in: capping layers using oleophilic ligands; water-soluble surface layers using hydrophilic ligands; bio-functionalities for targeting or therapeutic applications; versatile tether functionalities via selective reactions or interactions, figure adopted from [25]*

Surface ligands can have direct effects on the optical, electrical, magnetic and catalytic properties of QDs[7]. Often the aim is to preserve the QD luminescence, mid-gap trap states are then the first ones to be avoided. However, the relationship between ligand population saturation of surface sites and the electronic structure is quite unknown. One major open question arises from linking surface structure with optical properties[7]. Surface passivation upon ligand binding is common but not always necessary, some ligands introduce new mid-gap electronic states and increase the rate of non-radiative relaxations, which are undesirable decays. For example, alkanethiol ligands quench luminescence of CdSe QDs by fast hole trappings[7]. Ligands can also affect the energy barrier, which is for charges to hop between QDs. Long-chain surfactants enable a stable colloidal QD-solution. However, the ligands act as an insulating medium around the QD. These ligands are necessary to maintain colloidal stability in low boiling point organic solvents, but are detrimental to efficient electronic transport in QD solids, as they increase space between the QDs and lead to low film density[25][10].

Summarized, for improving film properties, ligand exchange and passivation of the surface prevent surface relaxation. It leads to further blueshift in absorption spectra relative to the bare QDs. Oxidation of QDs destroys the perfection of the QD surface, results in appearance

of an infrared adsorption band[26].

2.3 Characterization QDs

A wide variety of methods are used to investigate these physical properties. Among these methods are suitable techniques to characterize directly the shape, the size, the strain field of nanometer scaled structures and related defects[30], and optical parameters such as bandgap energy, PL, and lifetime. Coventional techniques for size and shape determination are Scanning Tunneling Microscopy (*STM*), Atomic Force Microscopy (*AFM*), Scanning Transmission Electron Microscopy (*STEM*), Energy Filtered Electron Microscopy (*EFTEM*). For absorption and emission measurement, common techniques are Ultraviolet-visible (*UV-vis*) and photoluminescence (*PL*) spectroscopy. Another important property is the lifetime of the QD emission. Lifetime is defined as the inverse of the PL decay rate, measurements can be performed with the Time-Correlated Single Photon Counting *(TCSPC)* technique. The used methods in this project are UV-vis, SEM, AFM, PL measurement and TCSPC, in particular to measure size, PL, lifetime before and after the exposure, in order to indicate the difference between the QDs before and after exposure.

In UV-vis spectroscopy, the sample is irradiated with the light spanning the UV and visible wavelength range and the electronic transition matching with the particular radiation is absorbed, the remaining light is passed through the sample and is observed. The obtained spectrum indicates the amount of absorbed photons at each wavelength of the UV and visible region of the electromagnetic spectrum, this is the absorption spectrum[16]. In the UV-vis spectrometer, the light source covers the entire visible and the near UV region(200 - 850 nm). The beam of light from the light source is then separated into its component wavelengths. One half of the beam (the sample beam) is directed through a transparent cell containing a solution of the QD compound being analysed, and other half of the beam is directed through an identical cell that contains the reference solvent or reference sample. Both these beams are collected by the detectors simultaneously and the absorption spectrum will be obtained, an example is given in figure 9.

The fluorescence emission profile also characterizes the size and shape of QDs, PL spectroscopy is a widely used technique for this. After absorption of photons, photo-excitation will be initiated. Of the various relaxation processes only one is radiative, the others are non-radiative where no photon is emitted. Time periods between absorption and emission vary for different inorganic semiconductors, for perovskites the range is in the nano-microsecond regime, for silicon even milliseconds[31]. The excited electron recombines with the hole by emission of a photon with an energy that corresponds to the bandgap. The bandgap can be fine-tuned by the size or shape and is a key parameter that determines the spectral position and purity of PL. For this project, the WITec microscope system is used to measure the PL. Examples of PbS absorption and emission spectra are shown in figure 9.

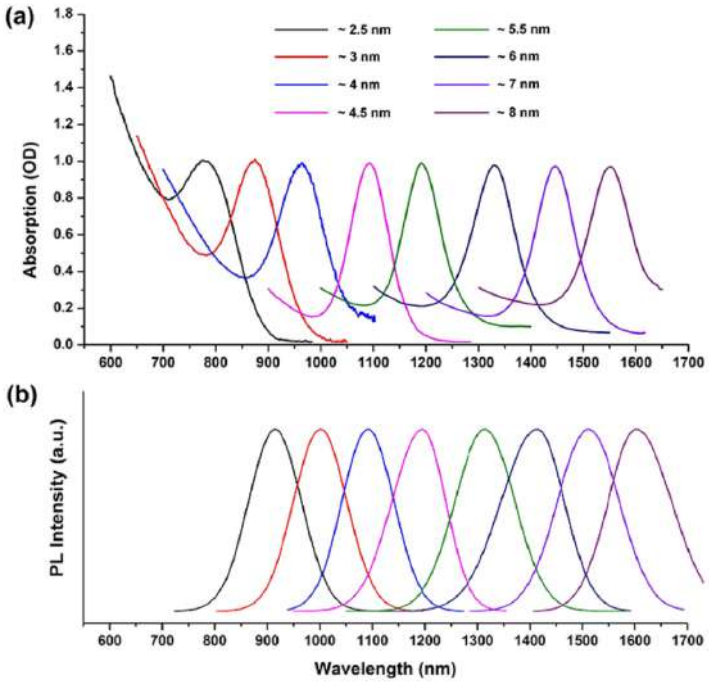

Figure 9: *Example of absorption and emission spectra of PbS QDs[32]*

Following the PL profile, the PL lifetime is measured through TCSPC, which measures the rate of fluorescence decays. The rate is an important property for energy or charge transfer purposes in a device. The technique of TCSPC uses a pulsed laser as light source of excitation, single photon events are detected and their time of arrival is correlated to the laser pulse. By using a pulsed laser with a high repetition rate, a photon distribution over a time period and the spatial coordinates can be built up. Then the relaxation from an excited state to a lower energy state of the QD can be analysed[33]. Since various QDs in a sample will emit photons at different times following their simultaneous excitation, the decay must be determined as having a certain rate rather than occurring at a specific time after excitation. To ensure that the decay is not biased to photons arriving early, also known as the "Pile-up" effect, that leads to a systematic underestimation of lifetimes, the photon count rate is kept low. According to literature [33][31], the rule of thumb is to have a photon count rate of 5% of the laser repetition rate, we typically use 1%.

By combining all the data points, an intensity versus time graph can be generated that displays the exponential decay curve referring to these processes[31]. However, it is difficult to analyze ensembles of QDs. One major complicating factor are the multiple energy states of many decay processes, thus multiple rate constants of different decays. Although non-linear least squared analysis can usually detect the different rate constants, determining the processes involved is often very difficult and requires the combination of multiple ultra-fast techniques[33][31].

2.4 E-beam lithography

This subsection covers relevant knowledge about e-beam in the context of this project. Starting with general information about the technology, subsequently the technical part of electron energy deposition and factors contributing to the resolution limit.

E-beam lithography is the practice of scanning a focused beam of electrons to draw structures on a surface covered with an electron-sensitive material, a photo or electron resist. The electron beam changes the solubility of the resist, enabling selective removal of either the exposed or non-exposed regions of the resist by immersing it in a solvent; developing. The resist either becomes soluble, allowing its removal by immersion in a solvent, this is called a positive resist. Or it becomes insoluble, making it resistant to a solvent so that the unexposed parts can be removed, this is called a negative resist[3]. The purpose, as with photolithography, is to create very small structures in the resist that can subsequently be transferred to the substrate material, often by etching[13]. A cross-section of an e-beam lithography machine is shown in figure 10.

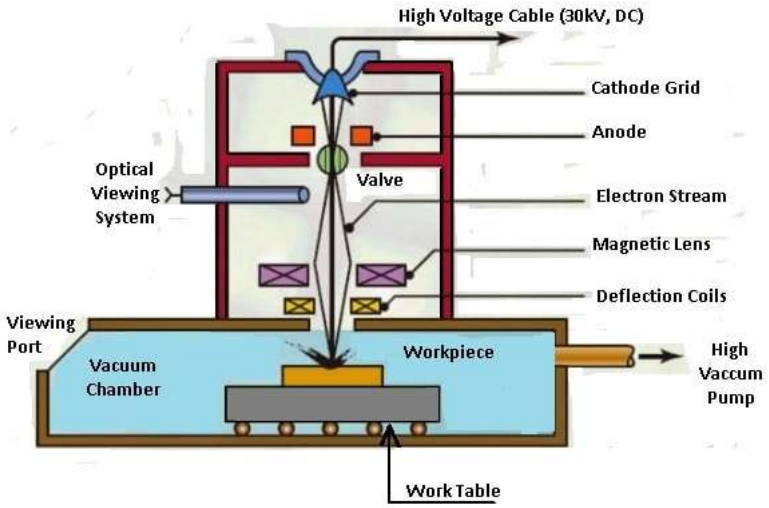

Figure 10: *Schematic cross-section of an e-beam lithography machine, with basic technical components indicated, figure adopted from [34].*

The primary advantage of electron-beam lithography over photolithography is that it can draw custom patterns in direct writing with sub-10 nm resolution. Electrons have shorter wavelength than photons, making them unaffected by the optical diffraction-limit[3], which is explained in section 2.4.2.

2.4.1 Electron energy deposition

Primary electrons from the incoming e-beam enter the resist through elastic and inelastic scattering, in other words they collide with other electrons. In such a collision the momentum transfer from the incident electron to an atomic electron can be expressed as:

$$dp = \frac{2e^2}{bv_e} \tag{1}$$

- e = elementary charge of $1eV = 1.602177 \cdot 10^{-19}C$
- b = distance of closest approach between the electrons
- v_e = incident electron velocity, defined by the voltage of the e-beam source

The energy transferred by the collision(E_{tr}) is given by:

$$E_{tr} = \frac{(dp)^2}{2m_e} = \frac{e^4}{E_{in}b^2} \tag{2}$$

- m_e = electron mass
- E_{in} = incident electron energy, given by the kinetic energy equation: $E_{in} = \frac{1}{2}m_e v_e^2$

When primary electrons are elastically scattered, the direction component of the velocity vector is changed and the magnitude is preserved since the kinetic energy is conserved. For inelastically scattered electrons, both direction and magnitude are changed. Most primary electrons lose their energy upon entering the resist atoms through inelastic collision and produce secondary electrons, these are capable of breaking bonds in the resist at a relatively long distance away from the original collision[35]. Moreover they can generate additional, lower energy electrons, resulting in an electron cascade, where free electrons are subjected to strong acceleration and subsequently collide with other atoms, thereby ionizing them[35][3]. Hence, it is important to recognize the significant contribution of secondary electrons to the spread of the energy deposition. An impression of electrons' energy deposition is given in figure 11.

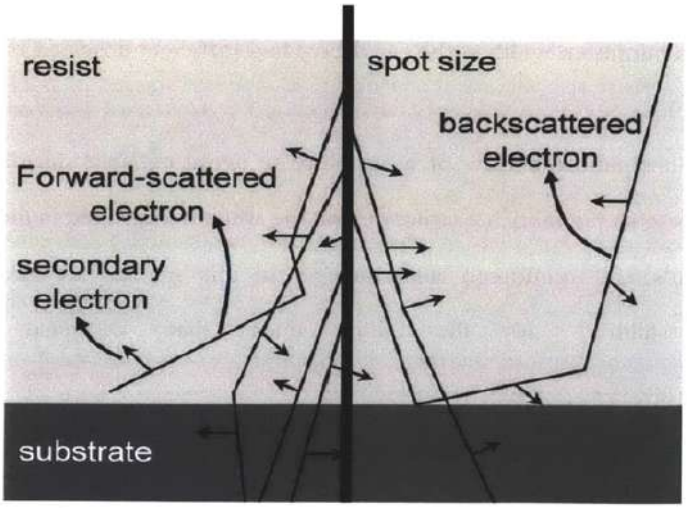

Figure 11: *Energy deposition of electrons in the material, figure adopted from [5]*

2.4.2 Resolution

E-beam lithography has been used through many decades. Although it is not suitable for large-scale applications, where photolithography is used, its resolution limit beats the diffraction limit of photons and allows features in the nanoscale regime. Wavelength of electrons is described by the de Broglie equation below, including the acceleration of electrons in an electron beam gun with the acceleration voltage:

$$E = q \cdot V = e \cdot V_{acc} = E_{kin} = \frac{1}{2} m_e v_e^2 \tag{3}$$

$$\Rightarrow v_e^2 = 2 \cdot \frac{e}{m_e} \cdot V_{acc} \tag{4}$$

$$\lambda = \frac{h}{p} = \frac{h}{m_e \cdot v_e} = \frac{h}{m_e \cdot \sqrt{2 \cdot \frac{e}{m_e} \cdot V_{acc}}} = \frac{h}{\sqrt{2 \cdot m_e \cdot e \cdot V_{acc}}} \tag{5}$$

- $h = 6.626070 \cdot 10^{-34} J \cdot s = 4.135668 \cdot 10^{-34} eV \cdot s$
- V_{acc} = acceleration voltage

The used e-beam machine is ***Raith Voyager***. Its acceleration voltage is fixed at 50 kV. The theoretical wavelength of electrons follows from formulas above. One can conclude that theoretical wavelength decreases as acceleration voltage increases, at 50 kV the Broglie wavelength of the electrons is:

$\lambda_{50kV} = 5.491 \cdot 10^{-12} m = 5.491 pm$

One disadvantage of e-beam lithography is their electron-scattering characteristics[35]. Even though it is possible to focus the beam of electrons down to a diameter of a few nanometers, a halo of much larger dimension is formed around the point of impact caused by the scattering in the resin material on the substrate. The resolution attainable is improved only by using very thin layers of the resists, due to the exposed diverging area by electron scattering. The resolution is rather limited by practical challenges, limiting factors to be addressed are spot size alignment, proximity effects such as electron scattering, secondary electron range in an area of the resist far away from the incoming electron beam. In the worst case, a strong widening of the focused electron beam may occur, which limits the resolution dramatically. It depends also on resist development, and resist chemical and mechanical structure[4]. Unfortunately, these limiting factors are not easily separable, leading to a challenging analysis. Therefore, understanding the effect of these individual limiting factors and the correlation between them is fundamental to drive e-beam lithography to the atomic scale of resolution.

The beam interacts with the resist as described before, secondary electrons deposit energy through the resist leading to resist cross-linking or breaking molecular bonds required for exposure. Additionally, electrons can backscatter out of the resist. The initial electron spot size may limit minimum feature size and, if broad enough, affects the minimum pitch and the periodicity of dense features. Sometimes, the incident electron may itself be backscattered as shown in figure 11 and leave the surface of the resist[13][35].

Many approaches have been used to investigate these factors limiting e-beam lithography, such as investigating different resists, varying electron beam spot size, varying electron energy, optimizing resist processing of before and post exposure, optimizing resist development, and simulating the deposited energy into resist.

This project focuses mainly on the following limiting factors: type of resist(the QDs), resist-substrate attachment, development conditions, and spot size, which is determined by structure design made with the Voyager.

2.4.3 Line Width Roughness(LWR) and Line Edge Roughness(LER)

Electric device performance is influenced by the uniformity of the line width of the transistor gate, and the line edge of features. A rough line can lead to yield loss or signal disturbance. Control of the line width roughness (*LWR*) and line edge roughness (*LER*) are thus critical issues in nanolithography, when features approach tens of nanometers. Figure 12 shows the LER and LWR of a straight line printed feature.

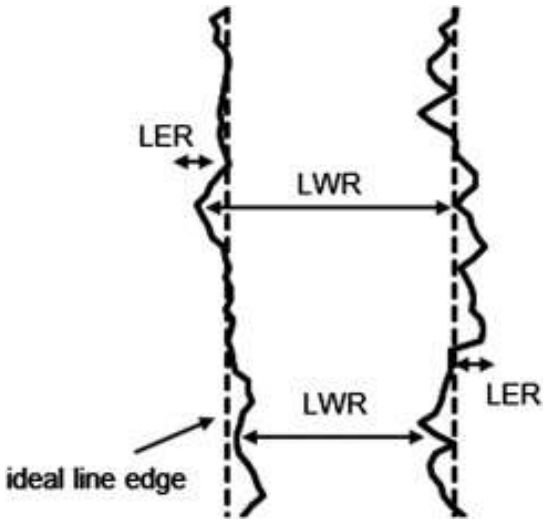

Figure 12: *LER and LWR indication of a straight pattern qualification[36].*

LER is defined as 3σ (standard) deviation of an edge from a line fit to that edge, LWR is the 3σ deviation of the width. Both LWR and LER will always occur in practice, this is caused by the material properties of the resist, post-lithography processing steps and shot noise[37]. The latter is related to the statistical behaviour of the irradiating particles that

enter the resist. Even when the resist properties, the projected image and the shot noise statistics are kept the same, many other factors influence the LER and LWR, the major challenge lies in isolating the relevant LER and LWR influence from the measurement method and the printing method. For this purpose, previous work has calculated the correlation between microscopy images and the influence of fundamental physical processes, by using computer simulations[35]. Finding resists with good sensitivity, good resolution and low LER and LWR is considered to be top priority for nanolithography and it therefore included in this project to look at the 3σ deviation of printed features.

2.5 Previous work

Not many reports have mentioned QDs as an emerging material for direct e-beam lithography. But it has gone through important developments as it has been demonstrated that it tunes further transformations on the QDs, leading to more complex patterns and thus major breakthroughs in nanofabrication that was until now impossible to obtain through other processes. This section summarizes the latest the findings on this topic.

2.5.1 Direct patterning nanocrystals

It was shown in the late 1990s that patterning nanocrystals can be applied for the fabrication of electrical circuits[38]. Later, patterned nanocrystals were used for detection of biological analytes such as proteins[12]. They were able to pattern features of micrometers on a QD film with e-beam. These results demonstrate the potential of the direct write lithography process on QD films for applications in bio-sensing. This was an example that showed the technological interest in combining the unique properties of colloidal nanocrystals with the large-scale versatile fabrication tools. Some of the previous works have specifically deposited nanocrystal in the desired areas of the substrate, but the spatial resolution that can be achieved by selective deposition is limited to the microscale.

Reetz et al. discovered that after e-beam irradiation on a nanocrystal film, the particles remained attached to the substrate. They concluded that e-beam irradiation had removed surface ligands and caused the consecutive aggregation in the exposed areas[12]. However, other groups questioned this explanation for insolubility after irradiation. First of all, the irradiation-induced anchoring was more efficient on nanocrystals capped with longer ligand molecules than shorter ones. This is consistent with the argument that anchoring occurs through cross-linking between the ligands, because of a higher probability of occurrence on longer molecules, and not through their removal, which would happen preferentially on shorter molecules. Additionally, characterization of the film after exposure and immersion in development solvent showed IR signal of the ligands and no reduction in film thickness. This suggests that the ligands were not stripped-off, but rather an induced cleavage of C-H bonds (dehydrogenation) and the formation of new C=C bonds, schematically shown in Figure

13b. To support this, a claim was made that carbon hybridization of capping ligands on a nanocrystal film goes from sp to sp^2 figure 13c,d), through X-ray photoelectron spectroscopy (XPS) and X-ray-excited Auger electron spectroscopy (XAES). Referring that C-H bonds are split and C=C bonds are formed[12, 39].

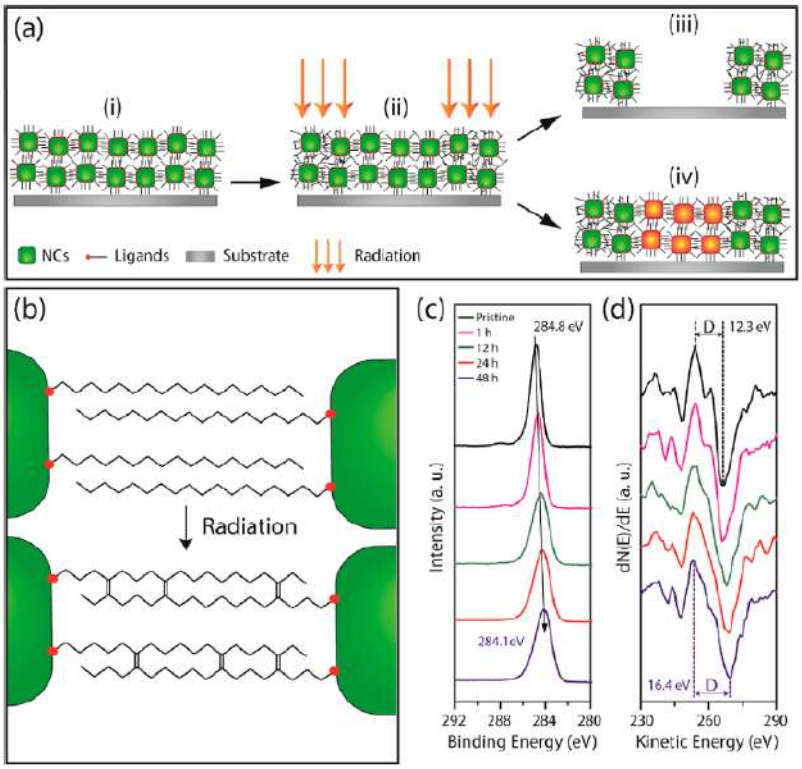

Figure 13: ***(a)*** *Visualisation of irradiation-induced patterning of colloidal QD films. Where QDs are deposited on a substrate, then the selected regions are irradiated and non-exposed regions are redispersed or selectively modified.* ***(b)*** *Irradiation-induced dehydrogenation and consecutive C=C cross-linking.* ***(c)*** *Evolution of the C 1s XPS spectrum and* ***(a)*** *Numerical derived D-parameter, which supposed to proof C=C bond formation.[12].*

The explanation presented by Werts et al. has been supportedd by later works [40, 41] to the extent that they rule out the initial hypothesis of ligand stripping.

2.5.2 Primary or secondary electrons

Concerning the e-beam process, previous works concluded that the generated secondary electrons in the substrate cause the cleavage of C-H bonds and subsequently forms C=C bonds. A supporting argument is that C=C were also formed when the substrate was exposed to X-rays, thus in the absence of a primary electron beam[38, 39]. Although it does not rule out that under e-beam lithography the primary beam could also induce the formation of C=C bonds. It is quite difficult to disentangle the role of the primary and

secondary electrons in the process. Bedson et al. demonstrated, by varying the thickness of resist on a substrate, that the secondary electron emission yield is much higher for the thicker layer, meaning that regions farther away from the primary beam spot are irradiated by secondary electrons.

2.5.3 Physicochemical transformations

There is some consensus in literature about the induced chemical changes in the ligands that cap the inorganic core. The question remains though as to whether the core themselves are affected by the irradiation. The data currently available suggest that, upon irradiation by e-beam, inorganic cores are not significantly affected, retaining their size, morphology, and crystallinity. process[39].

Another important aspect to consider is the evolution of the PLQY upon irradiation. As mentioned in section 2.2, the PLQY is affected by the quality of the surface. Therefore, it is reasonable to suggest that irradiation, which as preSviously discussed causes chemical modifications on the nanocrystals surface, may lead to the formation of surface trap states. These traps then can act as non-radiative recombination centers for excitons created at the QD cores, thus quenching the photoluminescence of the film. It has been shown for several types of nanocrystals that PL intensity of the film drops with exposure dose[42, 6, 12].

One of the few publications that resembles this project was done by Nandwana et al., they synthesized CdSe/ZnS QDs with trioctyl phosphine oxide($TOPO$) ligands and exposed them with e-beam at doses ranging from 100 to 8000 µC/cm^2, see figure 14.

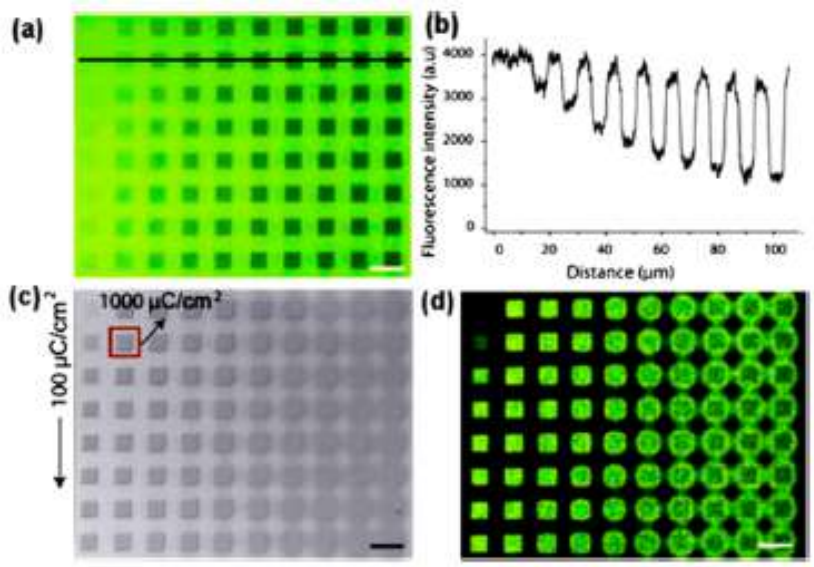

Figure 14: ***(a)****Fluorescent image of test pattern before development.* ***(b)****Fluorescence intensity across the patterns in panel (a).* ***(c)*** *Bright field;* ***(d)****fluorescent image of QD test pattern after washing with toluene. The dose varied* $100 - 8000 \mu C/cm^2$*. The scale bar is 10 mm[6].*

It was found that at very low dosages, the remaning PL was very weak and at very high dosages, stable patterns were not obtained due to overexposure by e-beam. The intensity map of developed test patterns shows the same pattern as unwashed sample except for low dosages where crosslinking was not sufficient to give stable QD features. They explored patterning of smaller QD nanostructures, features of 100 nm are fabricated without losing any film thickness. The fabrication of features smaller than 100 nm required higher e-beam doses, which lead to the degradation of the QDs. Their results suggested that the QD cores remain intact due to the remaining high PL after exposure, analogous to previous work. The e-beam presumably cross-linked the organic ligands present on the QDs. Between before and after exposure, there was hardly a difference in the position of emission peak and a small decrease in the intensity after patterning. Moreover, the QD films showed a negligible change in PL decay curves after exposure, indicating the preservation of discrete QD structures and no significant change in optical properties of these QDs. To extend this demonstration of direct patterning strategy that yields QD patterns with high resolution while retaining the optical properties, the aim of this project is to fabricate nanostructures smaller than 100 nm and explore more about the cross-link mechanism.

3 Experimental methods/measurements

This chapter explains the experimental methods used. First the CdSe synthesis, the PbS used were synthesized by other the Hybrid Solar Cells groupmembers. The second subsection explains the sample preparation. The CdSe QDs have been synthesized by the method of the daily supervisor Christian Dieleman, the synthesis of PbS was done by other members of the group before this project started. The quantities of all the chemicals are calculated to match the molar ratio for the products.

In the second part, the exposures and analyses methods are explained.

3.1 Synthesis CdSe: Hot-injection method

The Hot-injection method starts with the preparation of two precursors; selenium(Se), and cadmium (Cd). For Se-precursor, 0.1974 g of Se was placed into a Schlenk flask, followed by adding 25 mL of degassed octadecene(ODE). The solution stirred at 450 rpm while the flask was placed under vacuum. After the pressure had dropped to 0.6 mbar, the flask was filled with N_2. Temperature was increased to 180°C and it stirred for 5 hours. The solution ended up with the color of dark yellow to orange. For Cd-precursor, 0.0924 g of Cadmium-Oxide(CdO) and 24 mL of ODE were brought into a Schlenk flask, with 2.272 mL of oleic acid. The flask was flushed with N_2 and stirred at 450 rpm, at 100 °C, for 1 hour.

Then, the Cd precursor solution temperature had to be increased to 260 °C. At around 200 °C the solution became clear, as the CdO was dissolving. When the temperature approached exactly 260 °C, 7.2 mL of Se-ODE solution was added rapidly and QDs started to grow in the flask. Which lead to temperature decrease to 230 °C. Meanwhile the solution became clear and yellow, then it turned from yellow to orange to red. After a growth time of 5 minutes, the flask was moved from the heating mantle into cold water in order to quench the reaction. Figure 15 shows schematically the Hot-Injection method.

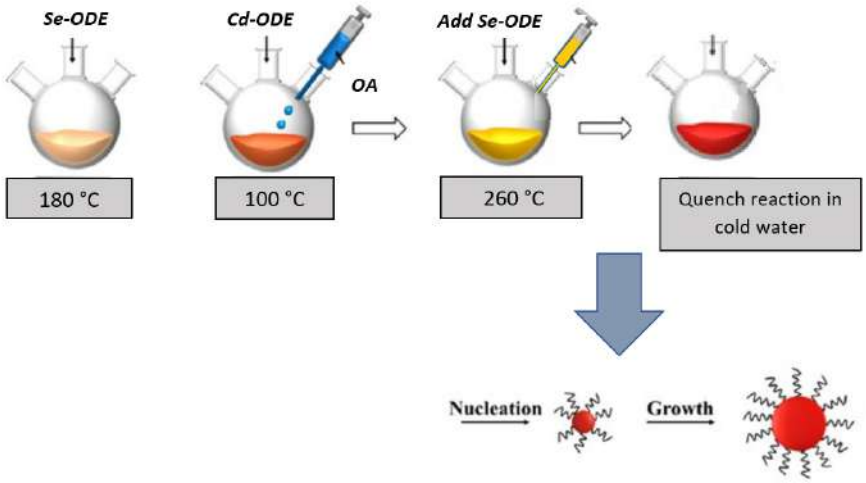

Figure 15: *Visualization of the Hot-Injection method*

After the flask was at room temperature, the QDs were purified with toluene and a mixture of iso-propanol(IPA) and methanol($MeOH$), ratio of the mixture is 1:1. This step was repeated till the QDs were precipitated and the solution was almost colorless instead of orange. The purification process ended up in a QD dispersion in toluene, this was dried overnight and finally the residual QDs yield was weighed. Desired concentrations of QD dispersion in octane were then prepared for depositing QDs on Si substrates, typical concentrations were 10 - 30 mg/ml.

3.2 Silicon substrates preparation

Silicon substrates of 12 x 12 mm were cleaned by toothbrush, soap and water, then sonicated for 20 minutes in acetone, and then IPA. Subsequently dried with N_2 gun, and placed into piranha acid (in volume percentage, 70 % Sulfuric acid, 30 % hydrogen peroxide). After 30 minutes in piranha, the substrates underwent O_2 plasma treatment for 15 minutes, to create a hydrophilic surface. But this hydrophilic surface activation is only temporarily stable, the duration of stability was measured by contact angle measurements in a Schlieren imaging set-up, shown in figure 16.

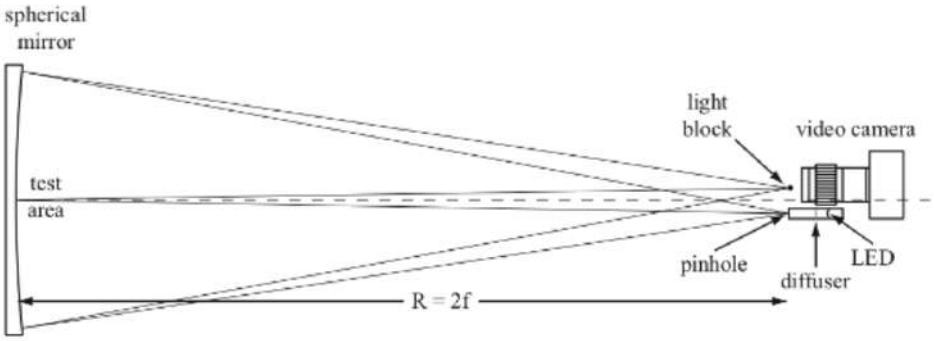

Figure 16: *The Schlieren imaging setup, including the spherical mirror, light source, light block, and video camera. The effect can be seen through the video camera[43].*

The QDs were deposited within the stable time of activated surface.

For the attachment of PbS, two different interlayers are applied, one type of linker-molecule *11-Mercaptoundecanoic acid* (MUDA) shown in figure 17, the other was an interlayer of sputtered gold.

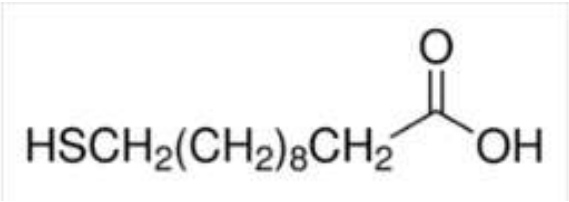

Figure 17: 11-Mercaptoundecanoic acid

For MUDA, Si substrates were soaked overnight in a solution of MUDA and ethanol, then dried with N_2 before depositing PbS. For gold, Si substrates were covered with 20 nm of gold by a sputter coater.

3.3 Deposition of QDs

The QDs were deposited on the substrate through spin-coating, in a N_2 glovebox environment ($O_2 < 0.1ppm, H_2 < 0.1ppm$). After two drops QD dispersion from the syringe on the substrate, the ramp-up time was 1.5 seconds, dwell time 30 seconds, and the rotational frequency was varied between 1500 and 3500 RPM during dwell time.

The thickness of a common spin-coated layer is proportional to the inverse of the square rooted angular velocity (ω), shown in equation 6, where T stands for thickness.

$$T \propto \frac{1}{\sqrt{\omega}} \tag{6}$$

The exact thickness of a layer depends upon the material concentration and solvent evaporation rate, which in turn depends upon the solvent viscosity, vapour pressure, temperature

and local humidity. Spin thickness curves are most commonly determined empirically[44]. In our case, the octane evaporated and the ideal thickness of QD layer was homogeneous and about 50 nm.

3.4 E-beam - Voyager

The e-beam tool used for nanolithography is a Raith Voyager based in the AMOLF NanoLab. As mentioned in section 2.4.2, the acceleration voltage of the electrons is fixed at 50 kV, the column mode is chosen at which the beam current is 0.133 nA, the dose is the variable parameter of this setting and is calculated according to:

$$Dose[\frac{\mu C}{cm^2}] = \frac{(beamcurrent[\mu A] \cdot dwelltime[\mu s])}{(step \quad size \quad area[cm^2])} \tag{7}$$

Therefore, under the same acceleration voltage, the energy of the incoming electrons per area is:

$$Energy[\frac{J}{cm^2}] = Dose[\frac{C}{cm^2}] \cdot Volt[V] \tag{8}$$

3.5 Development

After exposure, the substrates are developed for 10 seconds in a blended development solvent of toluene and IPA, at ratio $3:1$. And then cleaned with IPA, dried with N_2 airgun.

4 Results & discussion

In this chapter, relevant steps of the process are highlighted, including related data processing and discussion. Starting with a simulation of e-beam interactions with the substrate, made in the *CASINO*-program, the electron distribution is visualized. Thereafter the pattern design is shown, it is made in *Voyager Nanosuite 7.1* and designed to expose different doses and thin lines. Then the results of experiment optimization is explained; first the optimized QD attachment through Si surface activation, and then the substrate development. Finally, results of the structures are supported by SEM and AFM images, followed by PL characterizations(WITec) and lifetime measurements(TCSPC).

4.1 E-beam: CASINO & design

Before the experiments, we want to gain theoretical insight from electron distribution of an incoming electron beam. A simulation is made by using *CASINO*, a program based on Monte Carlo method for visualizing the trajectories of electrons in solid material. It is noteworthy that Monte Carlo is a stochastic estimation procedure, implying using random independent variables[45, 46]. According to state-of-the-art research, this continuum approximation approach of the average values is less accurate in real lithography events. The lengths scales between the gun and resist are so small that any shot noise can cause significant fluctuations[47]. These fluctuations in generated resist reactants or the absorbed energy can affect the lithography precision. Moreover, energy and momentum are spatially redistributed in resist by discrete, scattering low-energy electrons, producing image degradation[35, 46]. But since we only look at the ratio of energy distribution approximately, to gain clues about contributing factors of the resolution limit and cross-linking mechanism, we assume the Monte Carlo method is reliable to provide this estimation. Details of electron distribution mechanism such as phonons and the so-called point spread function[35] is beyond the scope of this project.

In CASINO, the chemical composition of the sample is set by regions, which in our case has multiple elements and a roughly estimated mass density of 280 g/mol (value taken from similar QDs of *Sigma Aldrich*). The thickness of QD layer is approximately 40 - 45 nm on a substrate of 12 mm $\times$ 12 mm. The used CdSe and PbS QDs have diameters of $\approx$ 5 nm and $\approx$ 3.4 nm respectively. The assumption is that all CdSe and PbS have these diameter values, and all toluene is evaporated during spin-coating. The QDs have a spherical shape, we also assume that they stack as spheres, leaving an estimation of 10 - 13 QDs on top of each other in the vertical axis. According to Aidan et al., the population of stearic acid ligand coverage on CdSe is 2.3 ligands per nm^2[48]. We take a smaller value of 2 for the OA ligands population due to the kink that OA contains, in contrast to stearic acid. By filling in the elements in CASINO, with the estimated amount of OA ligands and the total electron

energy of 312 keV (equal to a dose of $100\mu C/cm^2$ for $1nm^2$), the obtained visualization is given in figure 18.

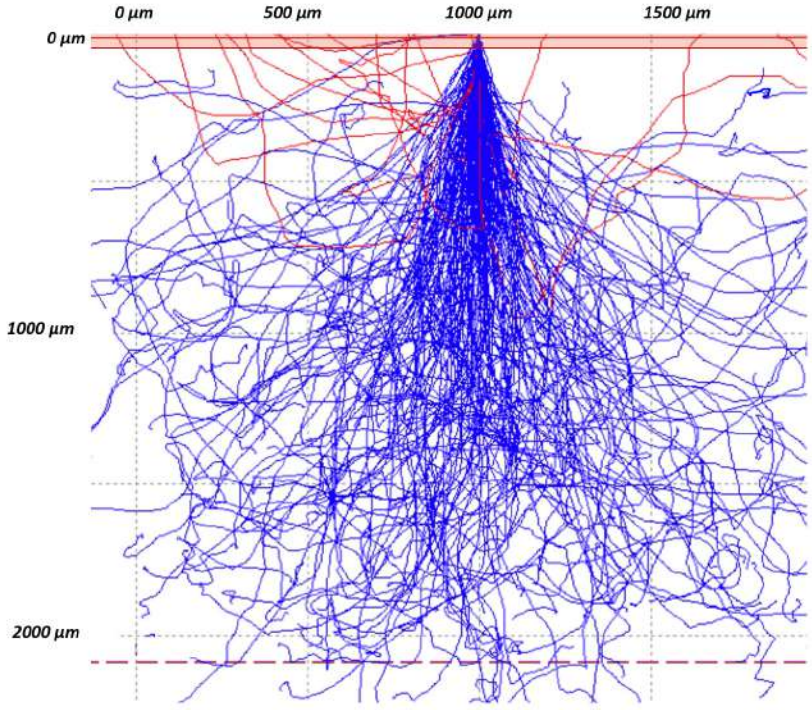

Figure 18: *Electron trajectories of a 312 keV beam, made in CASINO. Red tracks indicate the electrons that are backscattered out of the absorber, blue tracks are generated secondary electrons. One can see that the majority of the electrons go through the substrate due the high energy of the beam. The energy deposition in the thin layer QDs has a small surface range.*

Patterning the QDs starts with a design of the features. Figure 19 shows the design for nanoscaled stripes (upper half) and dose tests (lower half). The beam dosage is set on $30C/cm^2$ in the settings of Voyager, the numbers below every square indicate the exposed factor of this dosage. The dose test range starts from the lower left corner at 0.05(dark blue), which is equal to $0.05 \cdot 30\mu C/cm^2 = 1.5\mu C/cm^2$, till 8.70(red), equal to $261\mu C/cm^2$.

By filling in formula 8 with the used parameters in the Voyager settings, the obtained calculation is:

$$30\mu C/cm^2 \cdot 50000V = 1.5 \quad J/cm^2 \tag{9}$$

$$\Rightarrow 1.5 \cdot 10^{-14} J/nm^2 \cdot 6.242 \cdot 10^{-18} = 93.63 \quad keV/nm^2 \tag{10}$$

This is the setting at default for this project. The design for the substrate is shown in figure 19.

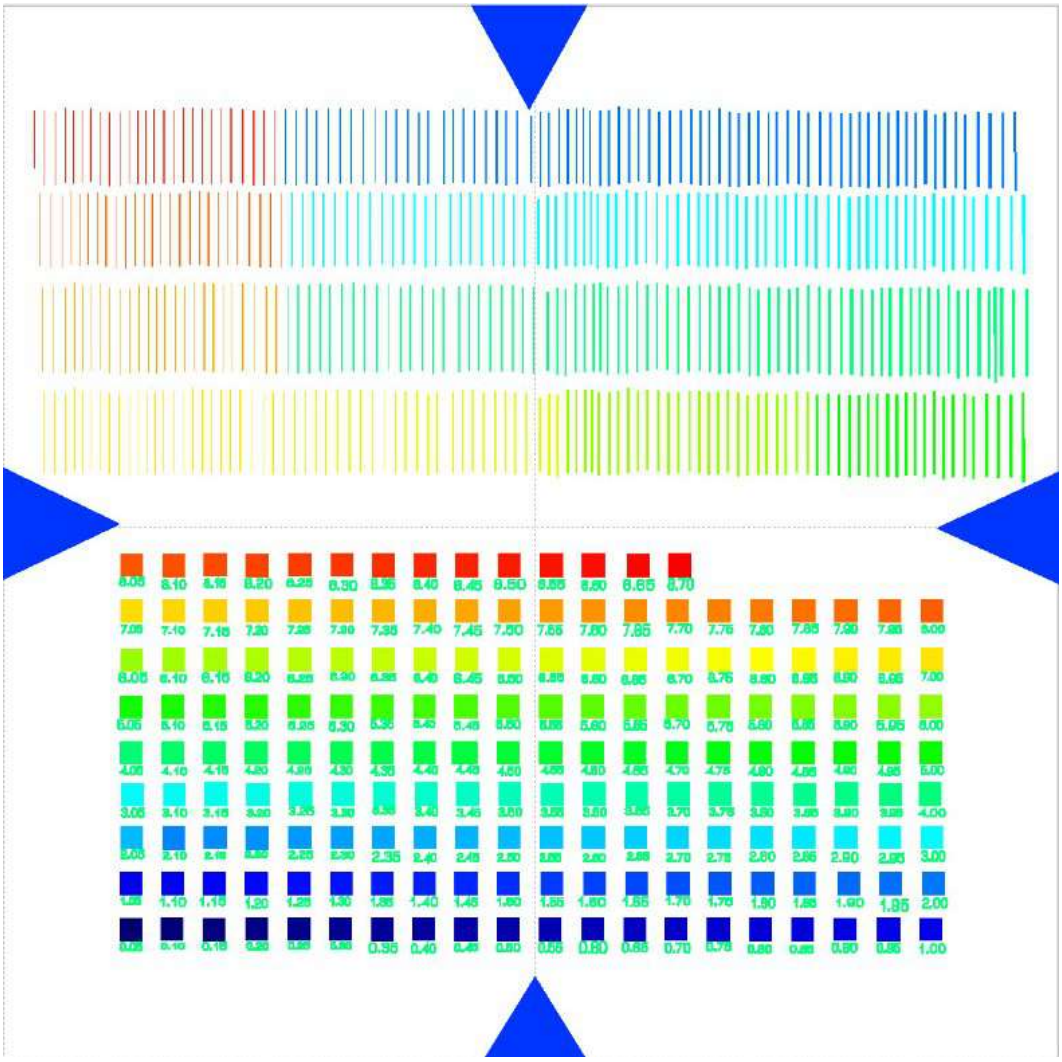

Figure 19: *Design for dose test with Voyager.*

The widths of the lines vary from 20 nm to 1000 nm at 16 different dose ranges, to test the resolution limit for these ranges. The attached doses correspond to the same colour of the squared doses, which vary from 0.05 to 8.70. By increasing the dose gradually, we can compare the exposed squares and lines.

4.2 Si substrate preparation

The first step of the experimental part is to prepare the substrates by surface activation, this is a crucial step for the QDs to attach during spin-coating as homogeneously as possible. Before depositing the QDs, Si substrates undergo oxygen plasma treatment, to improve the wetting of the substrate, thus the attachment between QD ligands and surface of Si. Oxygen plasma induces chemical bonding modifications for Si surfaces, leading to changes of contact angles[49]. Oxygen species such as O_2^- and O^- in oxygen plasma, are first absorbed onto the Si surface, and then they react with the Si–H groups on the surface to form Si–O–Si

bonds, as shown in the following reaction(figure 20:

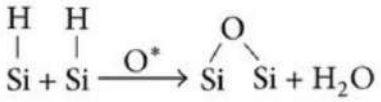

Figure 20:
Reaction of Si-H with oxygen plasma.

The Si–O–Si bonds spontaneously convert to polar Si–OH bonds once in contact with water in the conducted contact angle measurements, these Si–OH groups are extremely hydrophilic. As visible in figure21(a), the surface is extremely hydrophilic 5 minutes after plasma cleaning, the ultimate contact angle is below detection limit of 1°[50]. Figure 21 (b) shows that the substrate surface is less hydrophilic after 4 hours. Which explains a better attachment between H-atoms of the ligands and the O-atoms of the substrate.

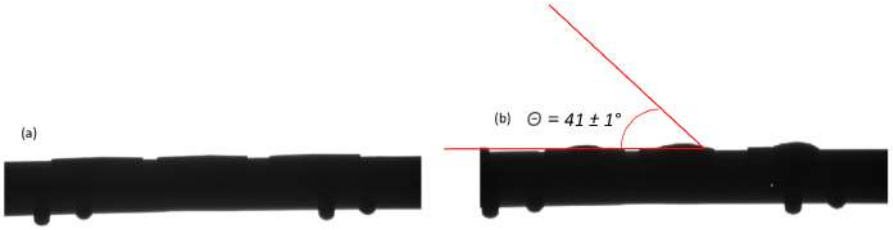

Figure 21: *(a) 5 min after plasma treatment; (b) 4 hours after plasma treatment.*

4.3 Optimal development

After exposure, the substrates are developed in a mixture of toluene and IPA with the ratio 3:1, this was an optimal combination between apolar and polar solvent. Since not all the QDs are altered in their structure during exposure, by using only toluene the development was too aggressive and the cross-linked QDs would also come off with other non-cross-linked QDs. Mixing toluene with the polar solvent IPA makes the development milder and prevents that the adjacent cross-linked QDs come off with the non-cross-linked ones.

4.4 Structures Characterizations: SEM & AFM

In this subsection, overall results of exposed CdSe and PbS are shown through SEM (***FEI Verios 460***) and AFM (***Veeco Dimension 3100 Bruker***) in tapping mode.

4.4.1 CdSe

For CdSe (12 mg/ml), the minimum dose where we can see contrast starts at factor 1.40, the color of exposed regions becomes darker as the dosage increases. Meaning that more

QDs remain on the substrate upon a higher exposure dose, see figures 23 and 22.

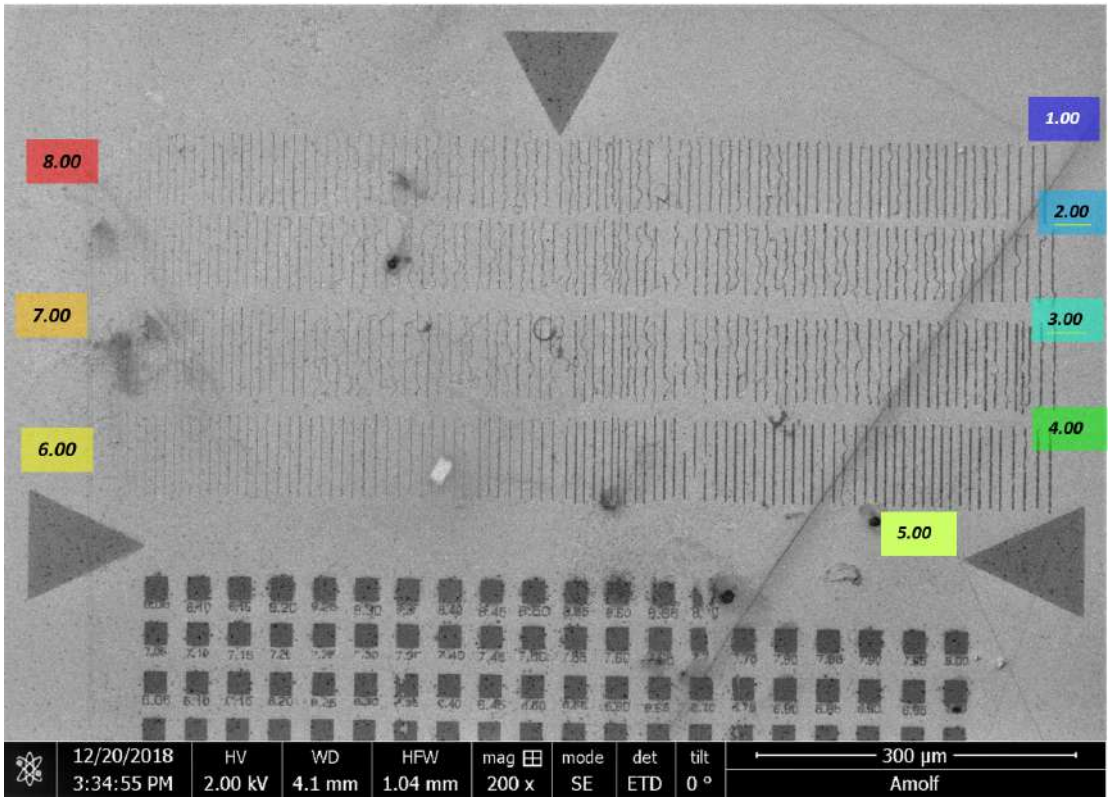

Figure 22: *Dose and lines CdSe 12mg/ml, upper half of the substrate, the colored boxes indicate factor regions, see figure 19 for exact factor locations.*

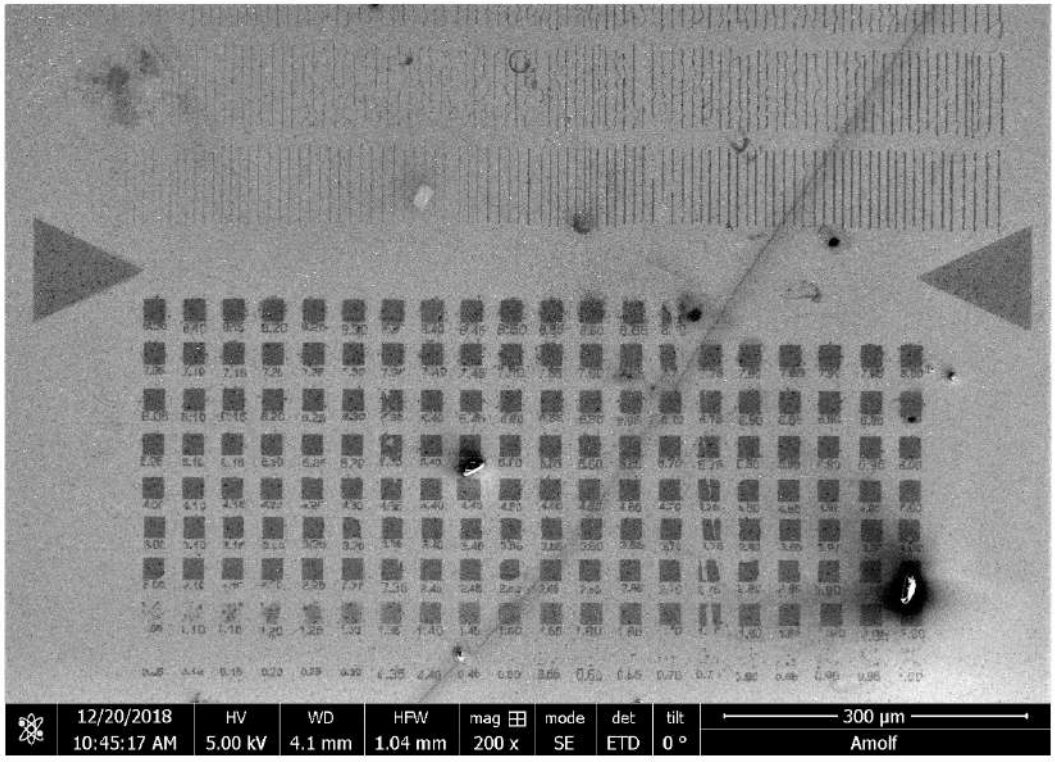

Figure 23: *Dose and lines CdSe 12mg/ml, bottom half of the substrate.*

Despite the insufficient attachment to the substrate and bad LWR and LER, lines down to ten of nanometers are visible. Figures 24 and 25 show zoomed-in regions from the substrate in figures 23 and 22. The thinnest visible lines are 20 nm thick, which is our smallest feature with lowest dose. When we compare 23 and 19, it is remarkable that thin lines are way more sensitive to higher doses than squares. In other words, small nano-structures tend to be overexposed, lines with a dose factor higher than 6.50 hardly remain, as we see on the left side of figure 22. Smaller structures need lower dose.

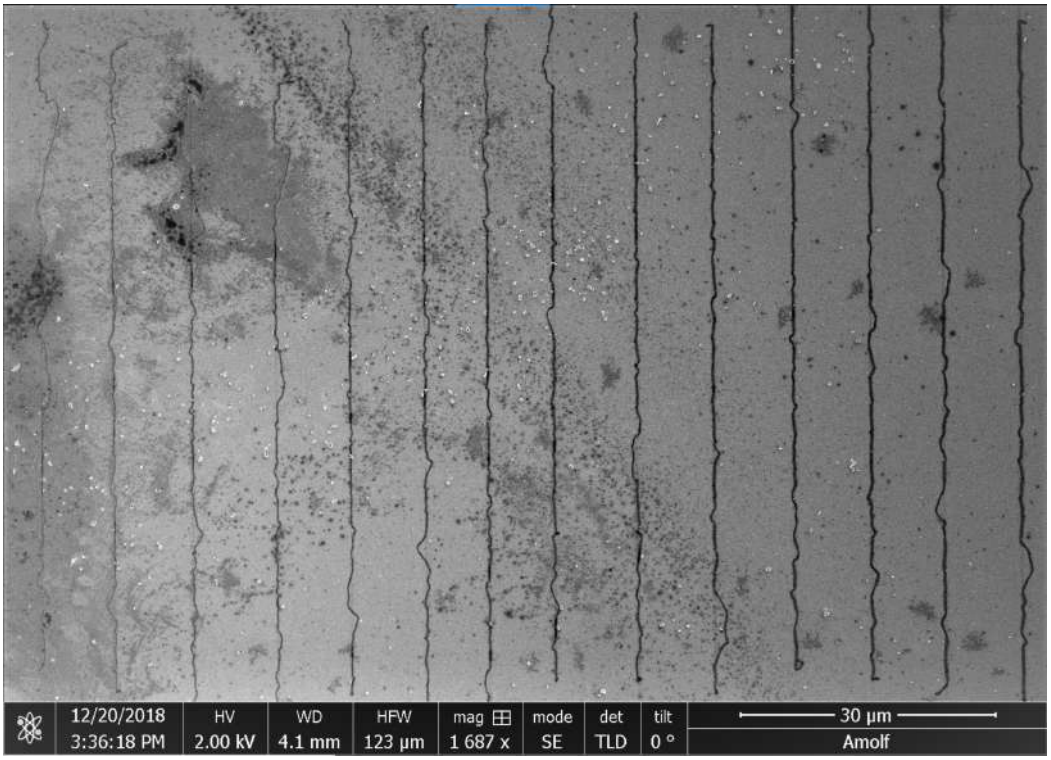

Figure 24: *Exposed lines of CdSe 12 mg/ml.*

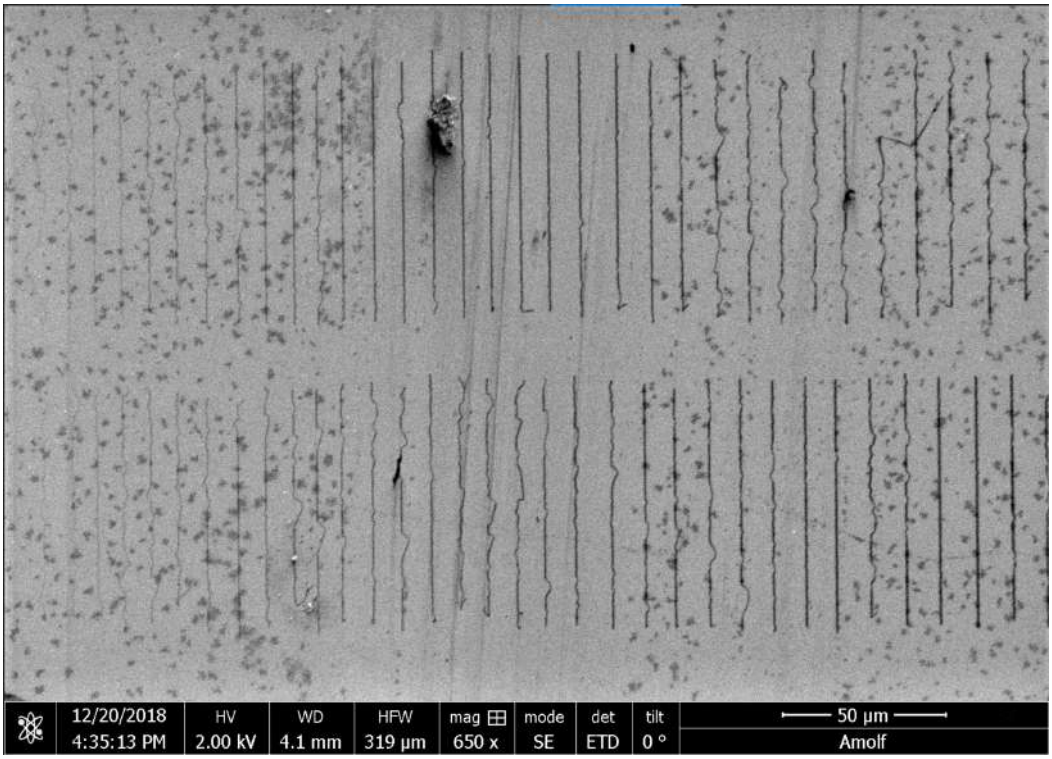

Figure 25: *CdSe 12 mg/ml, lines.*

When we look at the squares, the minimum needed dose is a threshold of rather a

continuous range. Probably because only a small fraction of QDs are modified by the electrons and remain on the substrate, or the initial film quality contributes such as the homogeneity. Part of the square is changed in its solubility, while the rest is dispersed during development, see figure 26.

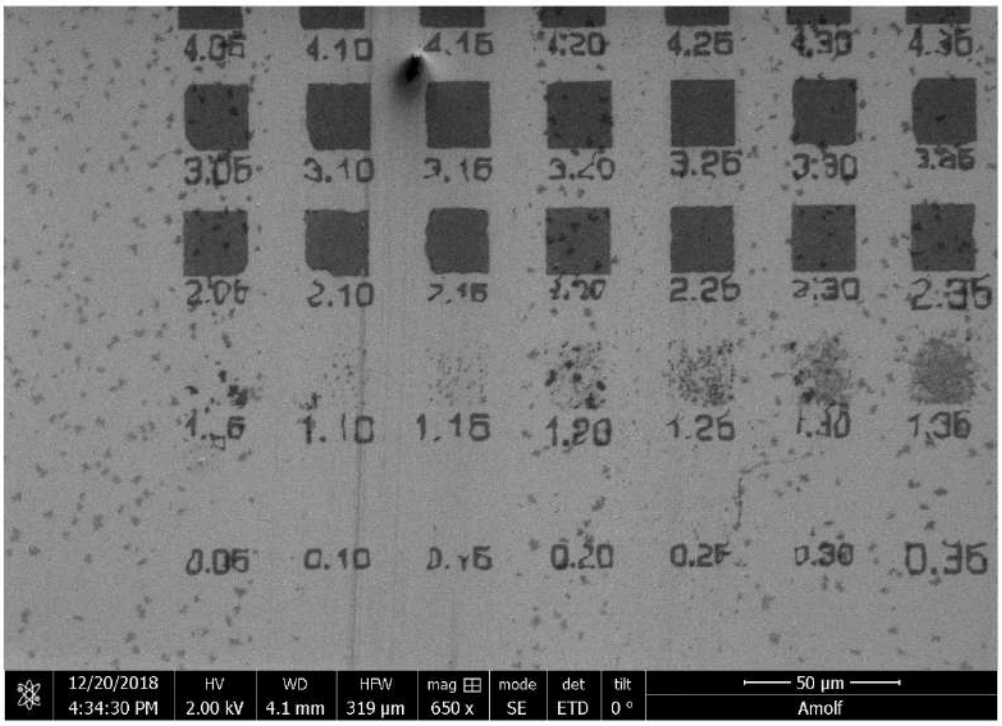

Figure 26: *CdSe 12mg/ml, the region of insufficient dose.*

This threshold is the same for CdSe films of 12 mg/ml and 13mg/ml, both are around 1.40 ($420\mu C/cm^2$) when we compare figures 26 and 27.

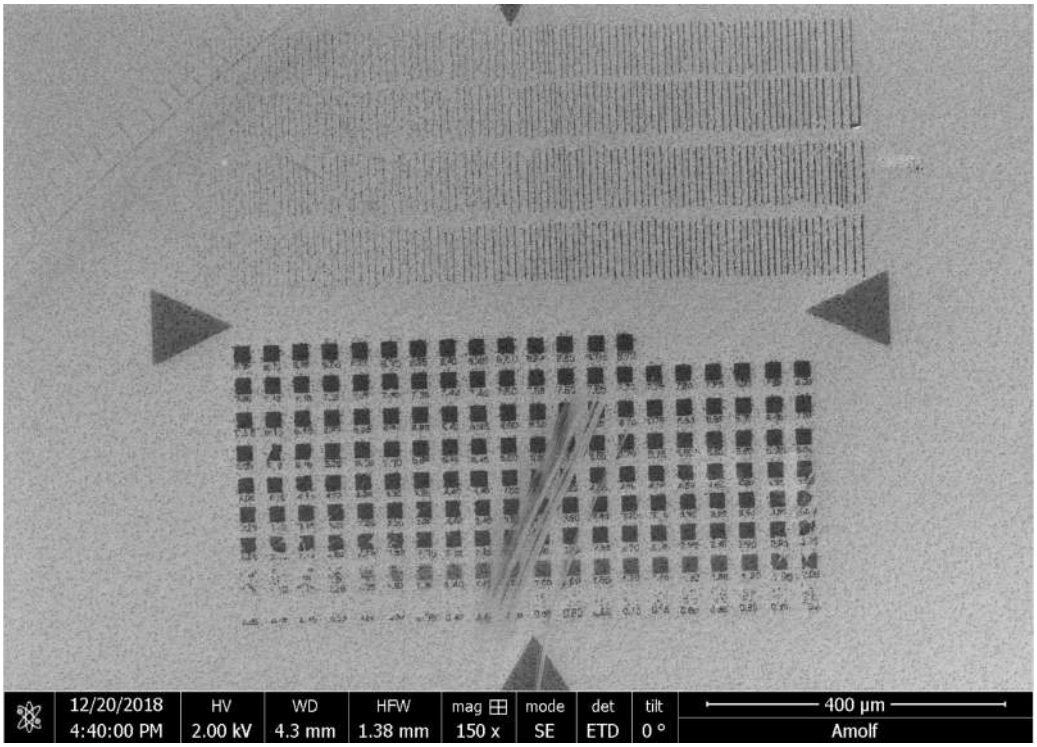

Figure 27: *CdSe 13mg/ml, dose test and lines*

For a higher concentration CdSe (18 mg/ml), the threshold is lower. Despite the contamination of the top layer in figure 28, we can see a whole square at 0.40 and at 0.50.

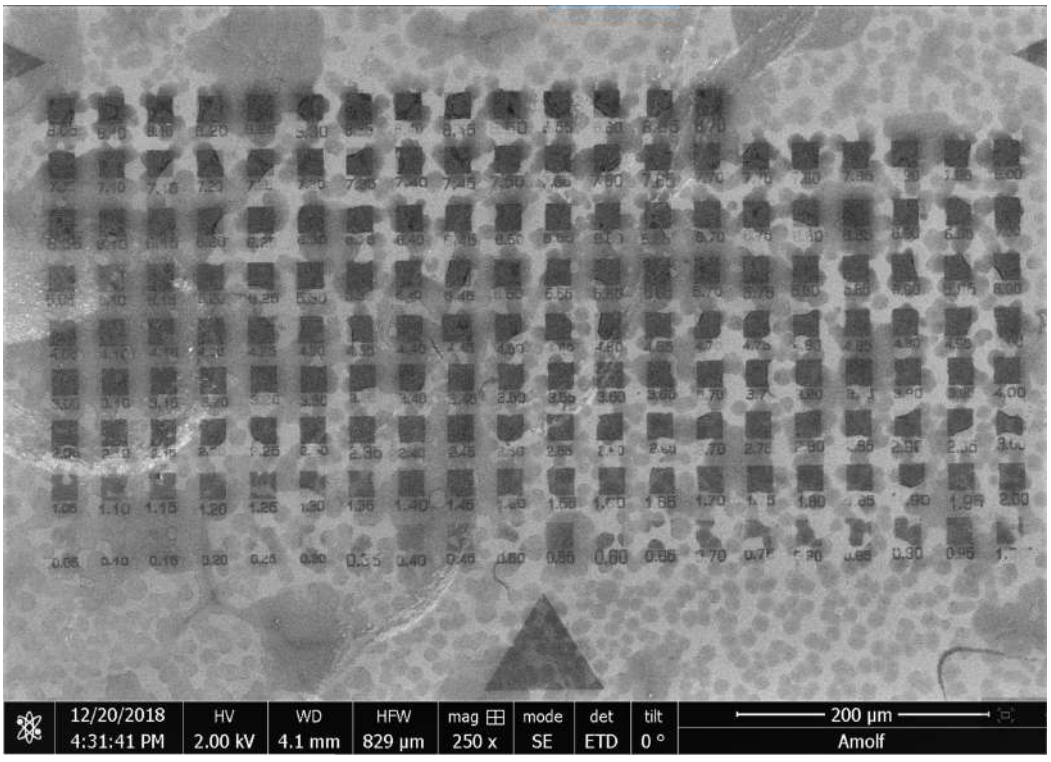

Figure 28: *CdSe 18mg/ml, unfortunately contaminated during development.*

So for this concentration, more QDs remain after exposure at lower doses. If there is a higher amount of QDs in the same area, a lower dose is needed as treshold to cross-link the QDs.

4.4.2 PbS

For PbS, the first results show a bad attachment between PbS and Si. Despite containing the same OA ligands, attachment is worse than CdSe, an interlayer of linking molecules are applied later on. Figure 29 shows the results without the interlayer, which are vague structures.

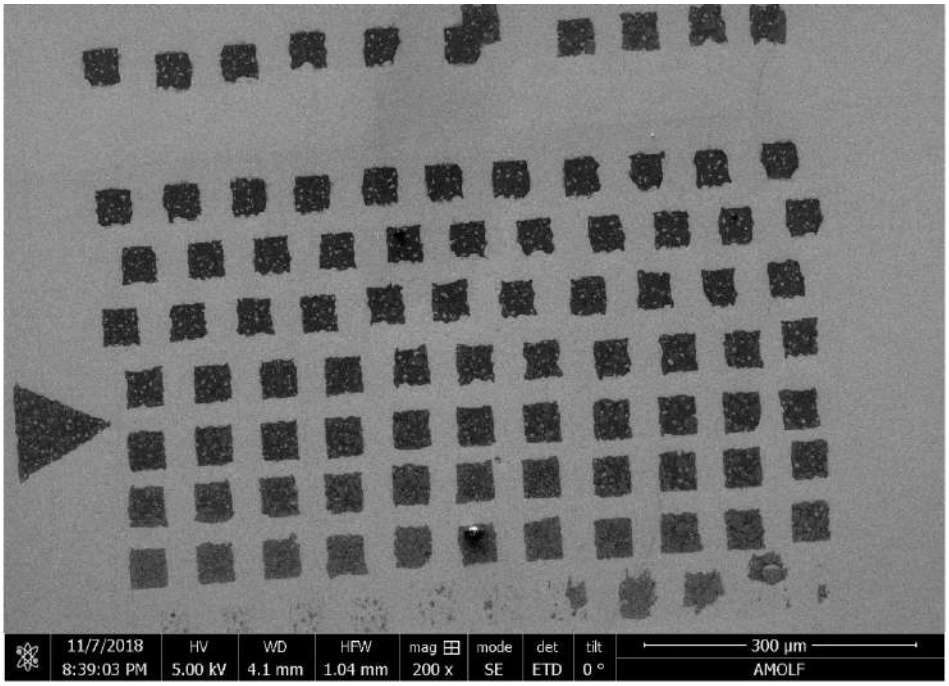

Figure 29: *PbS 15 mg/ml dose, without linker molecule*

From literature and experiments, we found that MUDA is a suitable linker molecule. It contains thiol (-SH) at the end of its long chain, in general thiols show the possibility of linking to metals and semiconductor via the strong affinity of sulfur that binds covalently. Thiols are also commonly used for creating system with which to accommodate the surface properties of several materials like metals, metaloxides and semiconductors[51]. The acid part binds to the PbS core, the molecule is long enough to bind both side between the core and OA ligands, figure 30 shows a successful attempt of PbS structures.

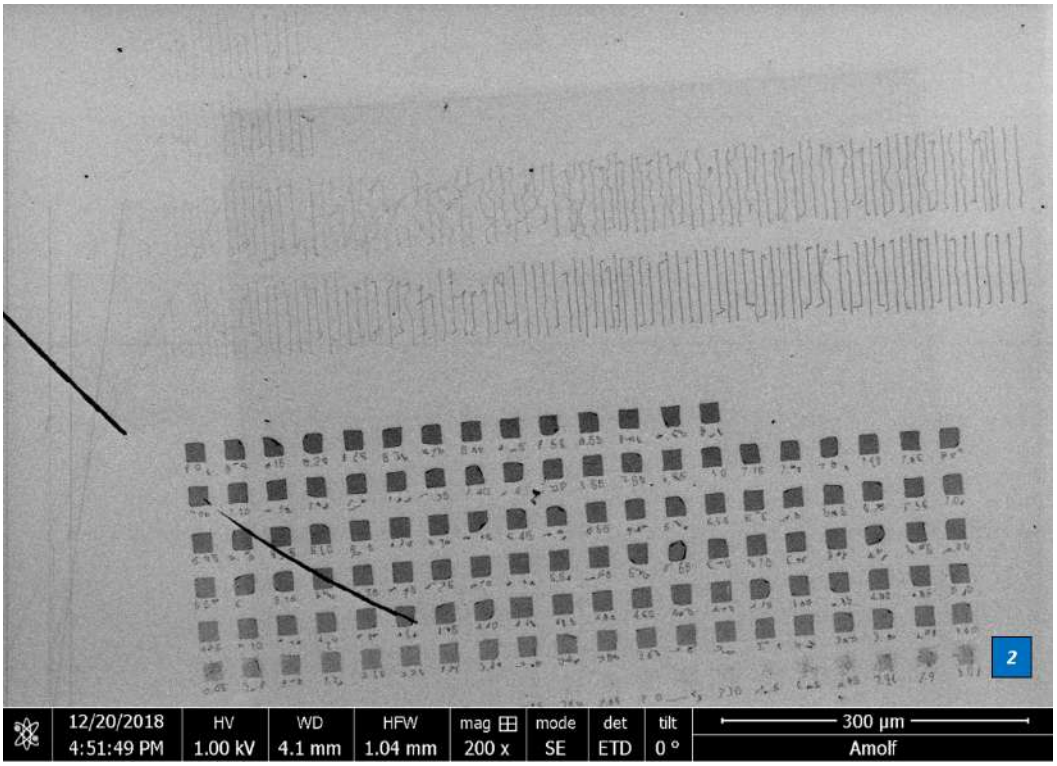

Figure 30: *PbS 10mg/ml, with MUDA.*

One can see that the threshold for PbS is higher than the treshold for CdSe, the row of dose 2 (indicated with blue square in the bottom right) is not visible in figure 30. It is difficult to distinguish which factors play a role. One hypothesis is that PbS has another sensitivity than CdSe, due to the smaller size and a lower bandgap energy. The measured emission peaks of PbS are at a higher wavelength, approximately 950 nm. Unfortunately these PbS measurements involved issues relating to accurate emission profile. According to literature the surface with organic ligands might cause oxidation of QDs, which destroys the perfection of the QD surface[26]. Since the PbS QDs are smaller, this oxidation-effect might be more significant. Another explanation is that the electron energy has also reached the MUDA molecules, leading to a less energy deposition in the QDs.

Figure 31 shows a zoomed-in region of 30-nm-lines at dose 3.50 ($105\mu C/cm^2$), the lines have remained but not totally on the substrate. Indicating a cross-link with other QDs, but bad attachment to substrate, so improvement is still needed.

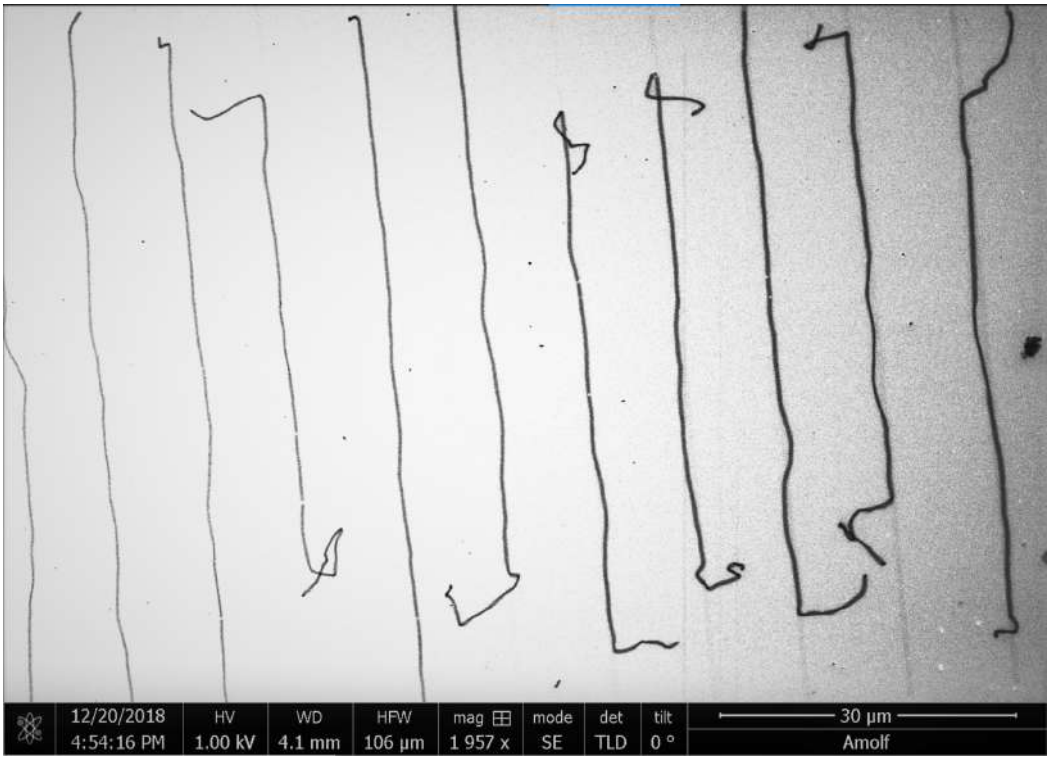

Figure 31: *PbS 10mg/ml, with MUDA, zoom-in on the lines.*

Besides applying linker molecule MUDA, we also sputter-coated an interlayer of Au between Si and MUDA. Due to a very strong binding between -SH and Au, results show a better attachment of the PbS to the substrate. However, the treshold of electron dose is even a little bit higher than with only MUDA. Which might be explained by the extra layer of thickness that take more energy from the electrons, resulting in threshold dose factor around 3.80 ($114\mu C/cm^2$) as visible in figure 32. Altough that layer is under the QDs, more scattering in between might have occurred.

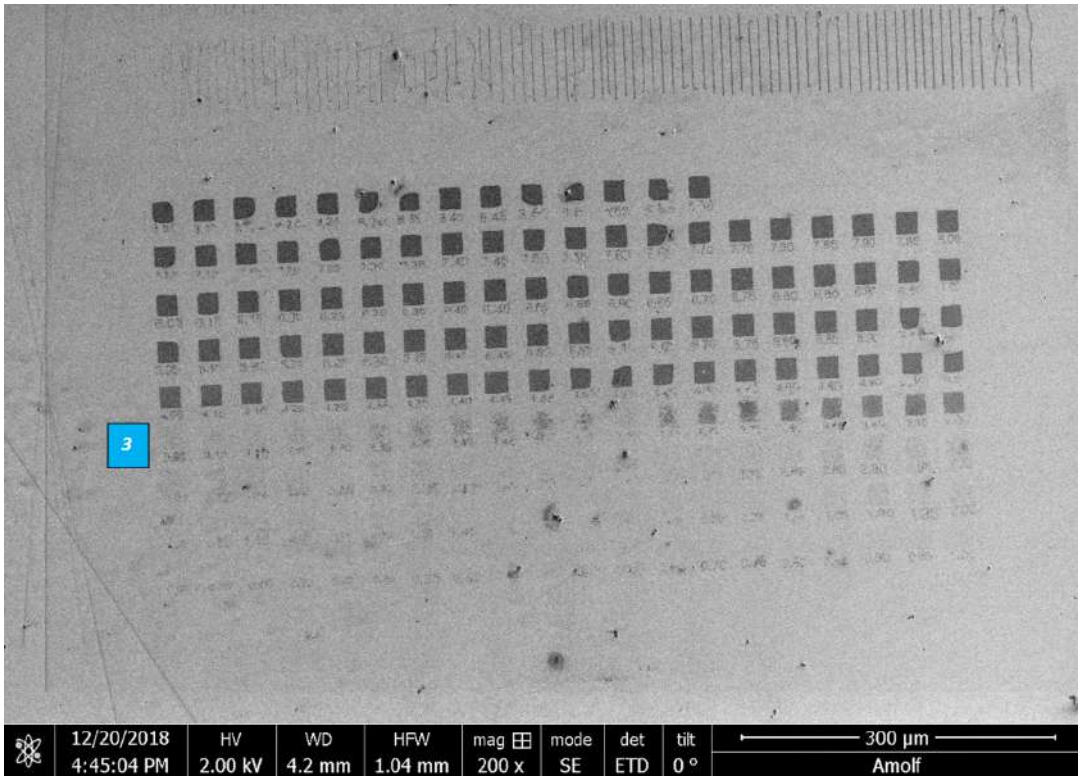

Figure 32: *PbS 10mg/ml, MUDA, 30 nm Au.*

As visible in figure 32, at the threshold of dose factor 3, the difference is more gradual than for CdSe. In other words, there is a bigger range with some remaining QDs visible at factor 3, for CdSe was this range smaller.

Figures 33 and 34 are zoomed-in images from 32, it shows the difference between the squares and lines, with only one dose factor difference.

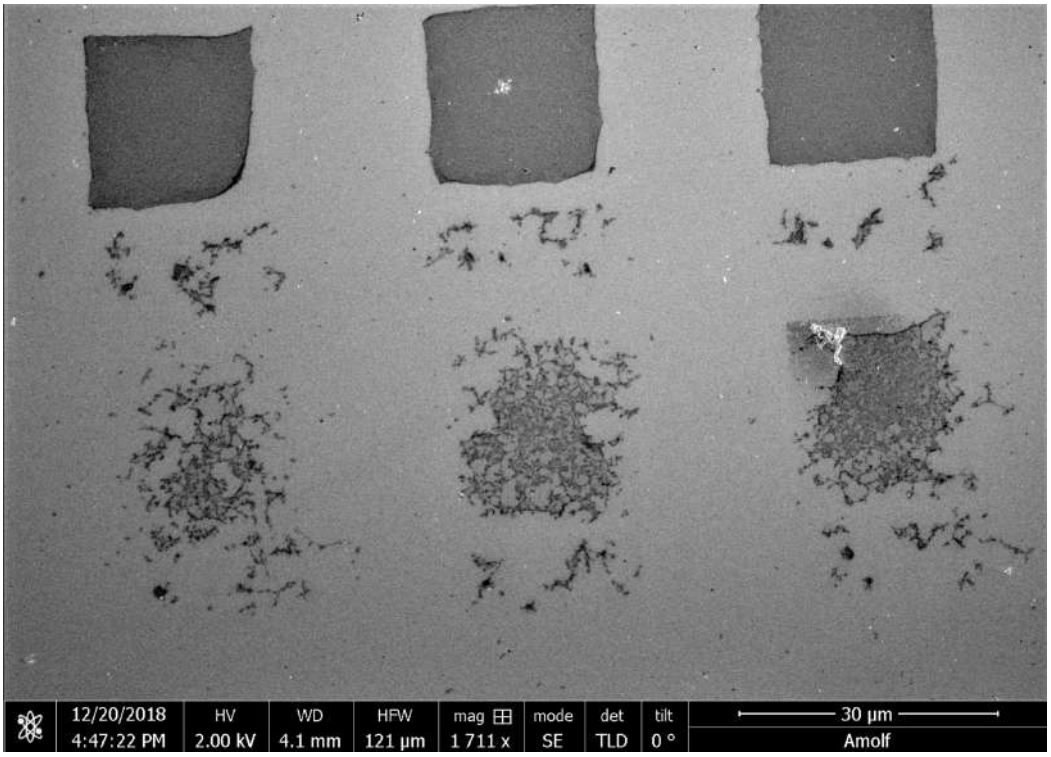

Figure 33: *PbS 10mg/ml, 30 nm Au, MUDA, zoom-in at the treshold where there is a big difference between factor 3.60 and 4.60.*

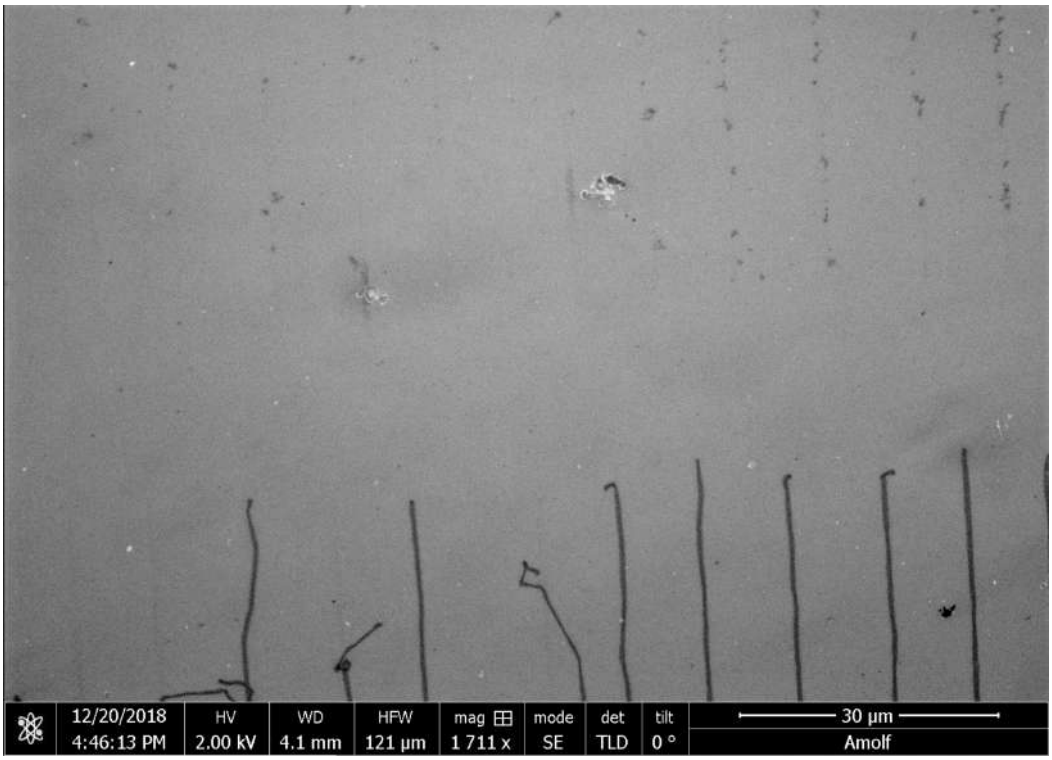

Figure 34: *PbS 10mg/ml, 30 nm Au, MUDA, zoom-in at the difference in factor 3.50 and 4.50 for lines.*

Figure 35 is another design that consists of small designs from the Voyager software, colors indicate different design layers and doses. We have exposed this to test accuracy with other designs.

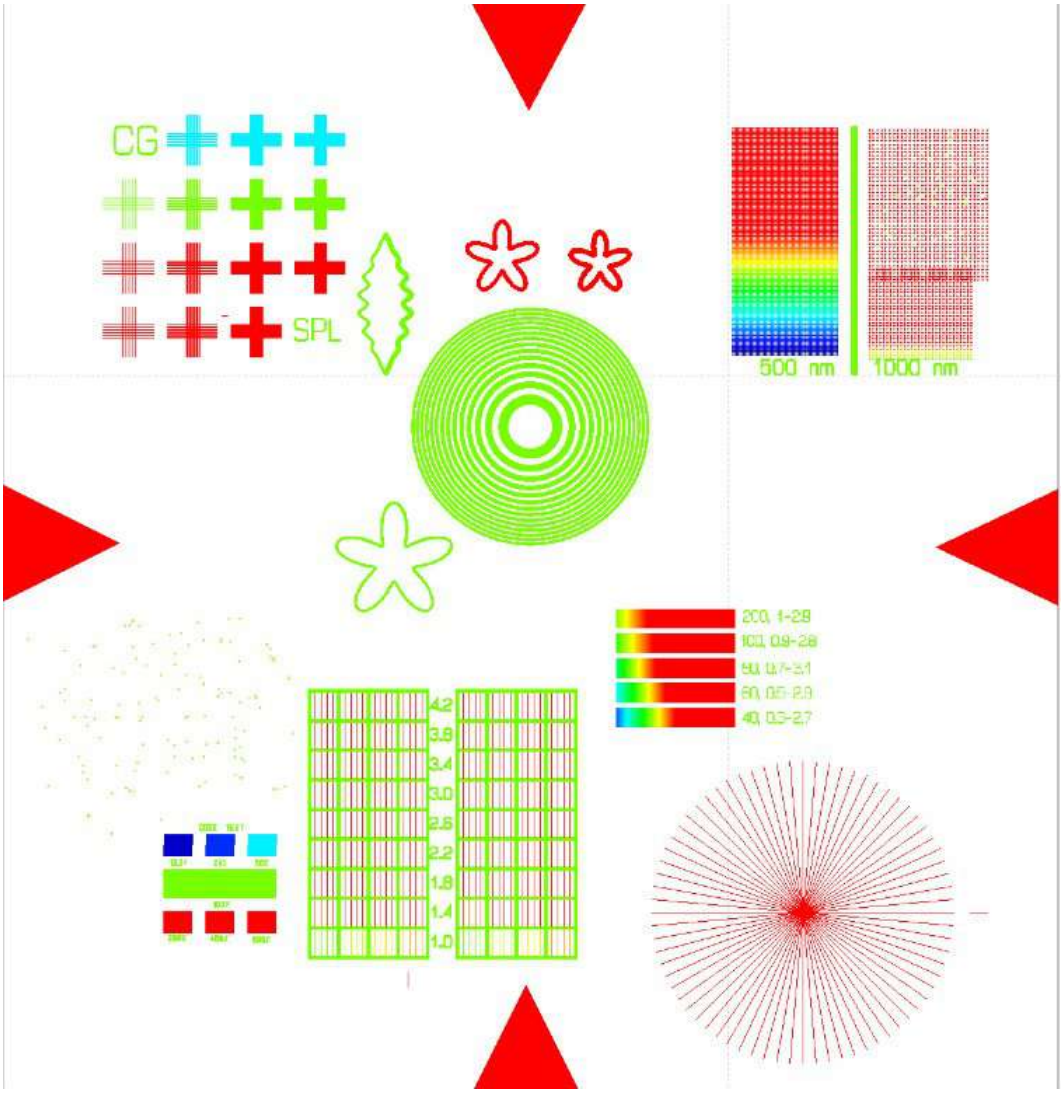

Figure 35: *Design Voyager.*

From an optimal CdSe concentration of 18 mg/ml and dose of $100\mu C/cm^2$, we succeed to fabricate nanostructures with low LWR and LER, as we see in figures 36, 37, and 38.

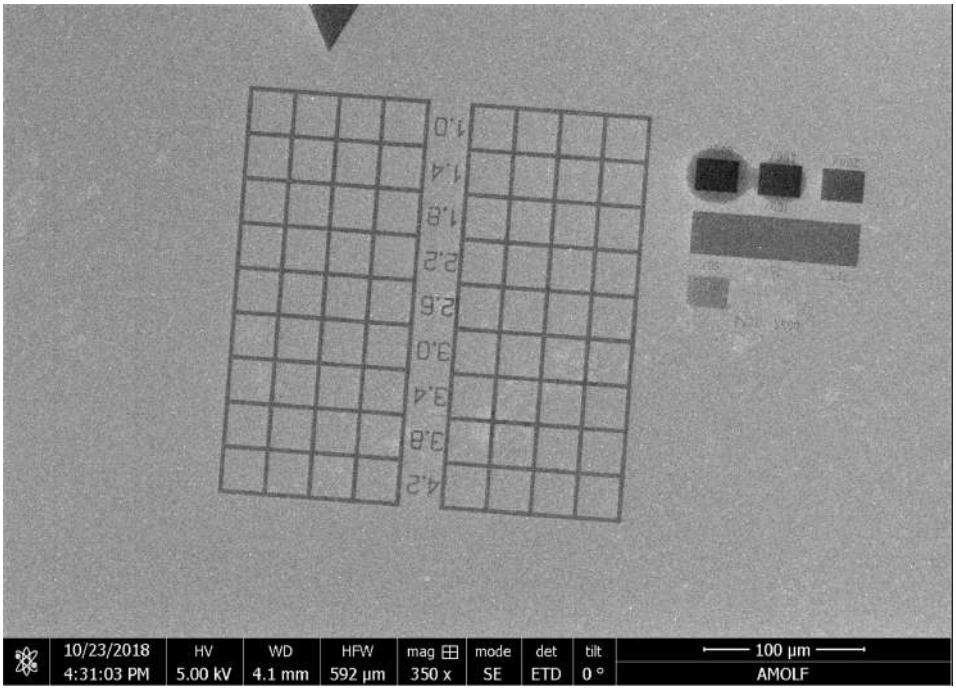

Figure 36: *CdSe 15 mg/ml, raster and dose test from Voyager design.*

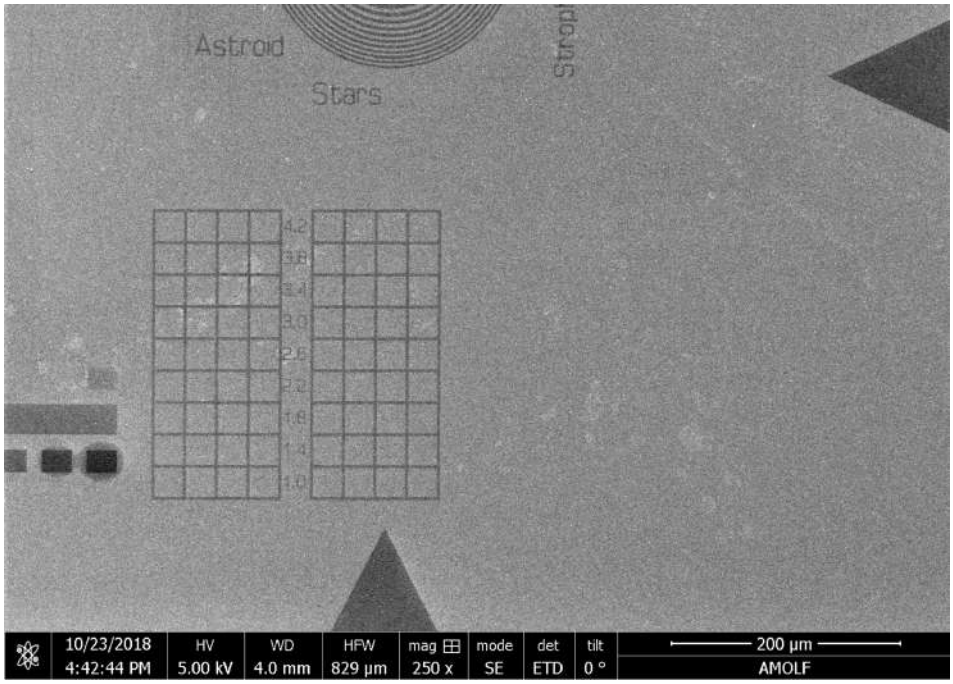

Figure 37: *CdSe 15 mg/ml, Voyager design.*

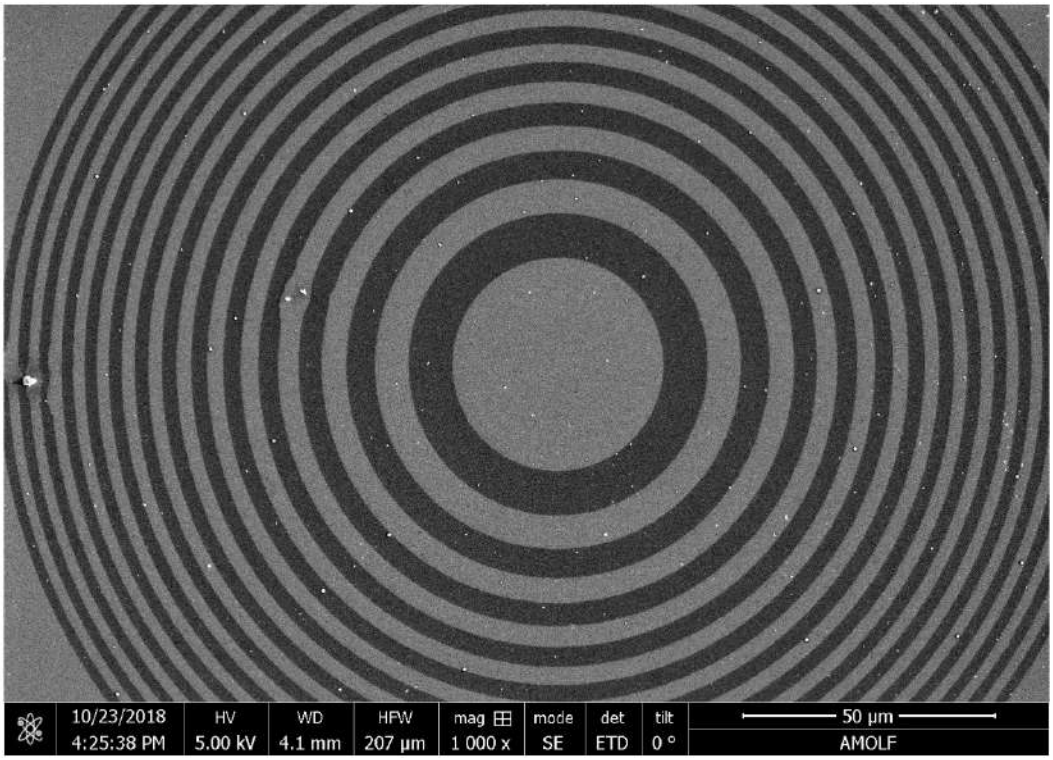

Figure 38: *CdSe 15 mg/ml, Fresnel structure.*

But for PbS, it remained difficult to obtain high precision structures, LWR and LER remained big issues, see figure 39. Improvements have to be made by optimizing surface attachment, or other concentrations of PbS dispersion.

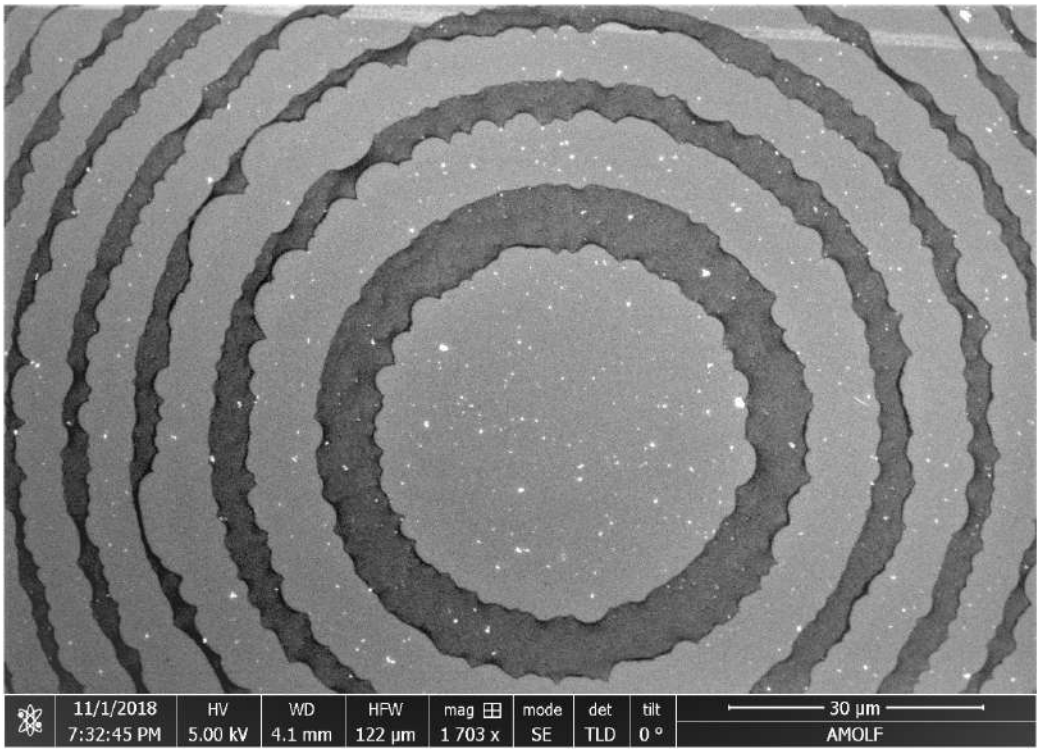

Figure 39: *PbS Fresnel structure.*

From this design, many parts contain a high dose, which was too much for our QDs, an example is shown in figure 40 and this looks similar to results from literature ref [12, 6].

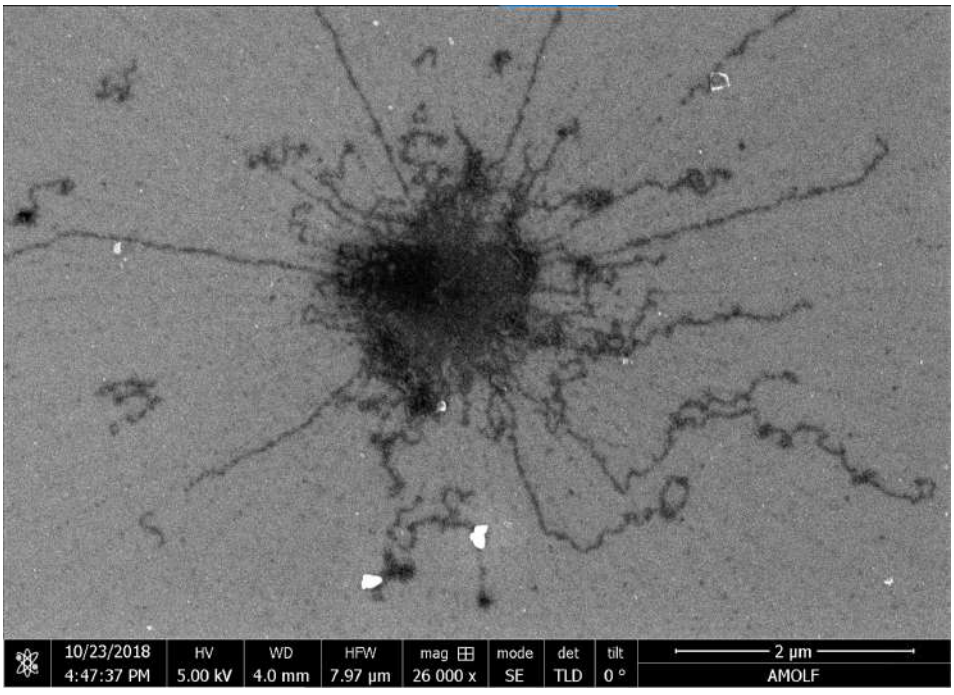

Figure 40: *An overexposed part of the design, the dose was too high and has modified the QD structure drastically. Similar to previous work of Nandwana et al. [6]*

A notable and unexpected result was the extremely stretched out lines, which provides good evidence for cross-linking, see figure 41. Since the length has stretched almost twice and it is for sure a line of QDs, no other explanation could be possible. There are no more QDs clustering in the stretched parts, they are thinner as we see from the SEM results. The QDs are more spreaded but still attached to other QDs. This could follow from cross-linking between the ligands of different QDs.

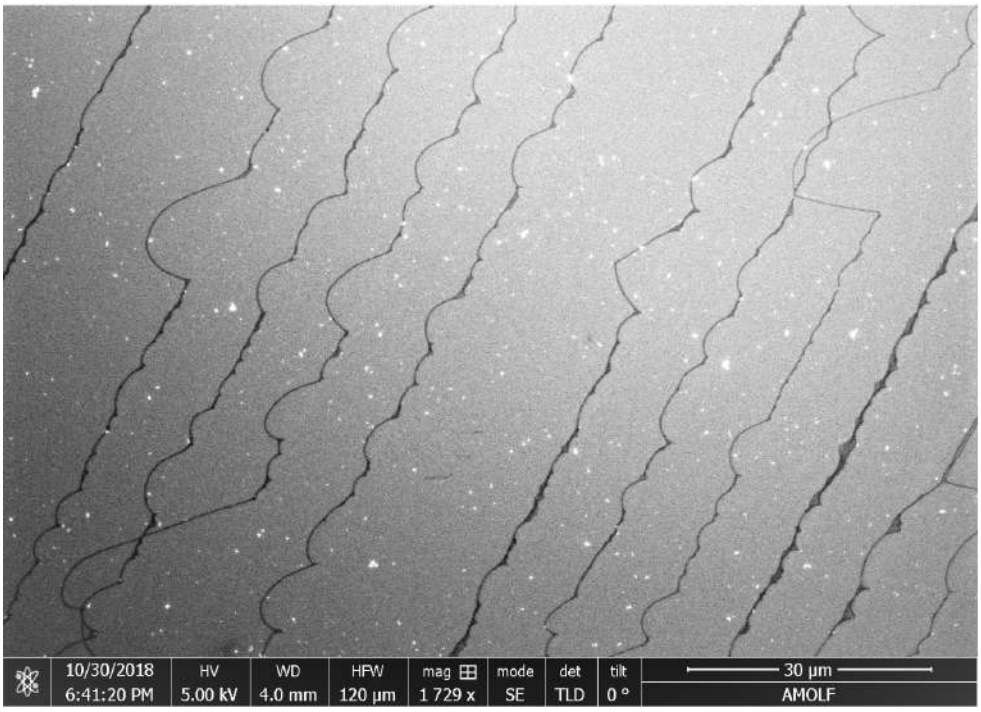

Figure 41: *Stretched-out QD lines.*

A cross-link is a newly formed covalent bond between different molecules. The OA ligand contain one sp^2(1 π - and 1 σ-bond) hybridization in the middle, the rest is sp(π-bond) hybridized. The bond energy of σ-bond is higher than π-bond, meaning that it takes more energy to break the σ-bond. But here, the incoming electrons have such a high kinetic energy that it would be possible for both σ and π to break. Localization of cross-links is difficult to detect, which is interesting for future work. In figure 42 an impression of possible cross-link scenario is shown between three QDs.

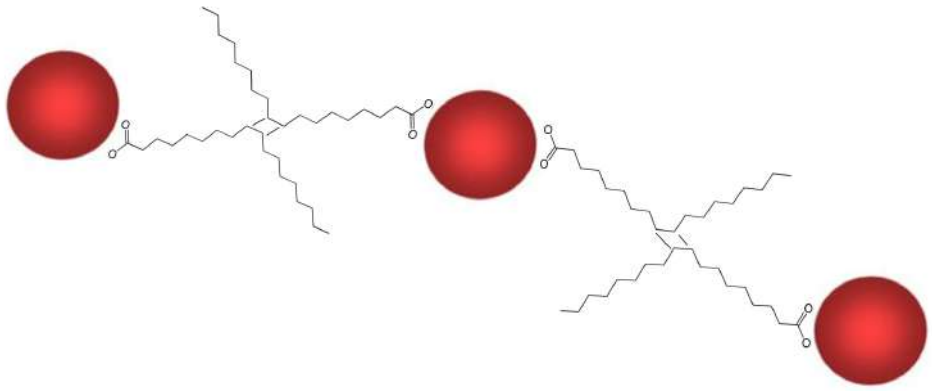

Figure 42: *Two OA ligands. During cross-link, covalent bonds(one electron pair) break and new covalent bonds are formed.*

For a 3D-visualization, the thickness of remained layer was measured through linescan of the AFM. Remaining QD layer is 10 - 15 nm, after the exposure dose of $100\mu C/cm^2$, see figure 43.

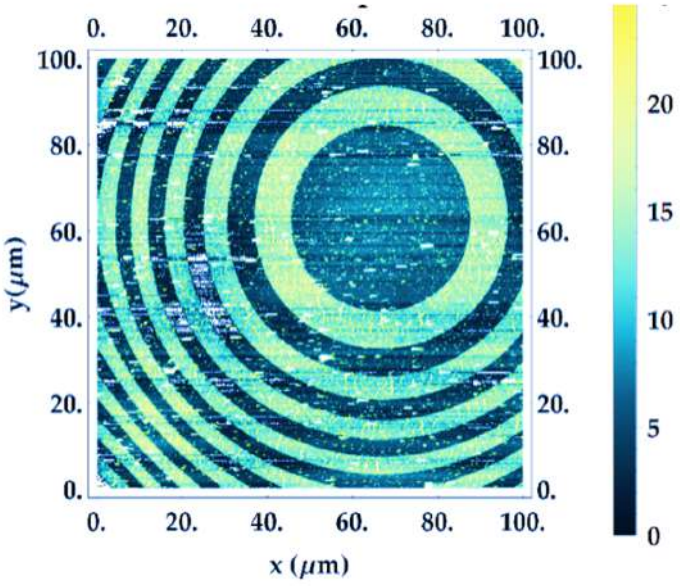

Figure 43: *CdSe 15 mg/ml, AFM map height map*

Figure 44 shows the cross-profile of Fresnel structure.

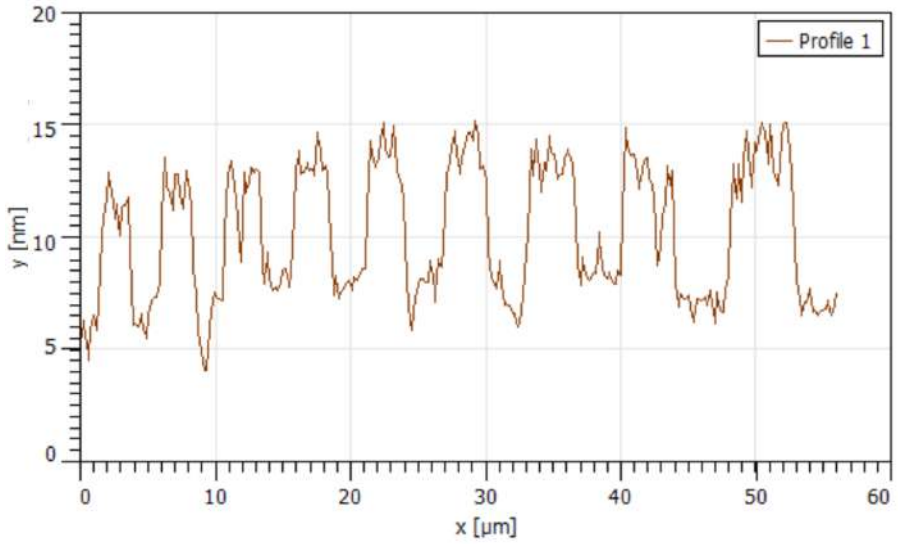

Figure 44: *AFM cross-profile of Fresnel structure.*

Compared to the thickness of the layer QDs before exposure(approximately 50 nm), there is only a small fraction left after exposure. Which could be a result of cross-linking, they can be closer to each other spatially due to overlapping cross-linked ligands next to each other. Another possible reason is a small loss on top of the QD layer, because mainly secondary electrons deposit their energy within the resist and a fraction of the primary electrons become backscattered out of the substrate. Therefore, the on top lying QDs do not cross-link and are washed away during development.

4.5 Luminescence Characterization: PL - WITec

For PL measurement, the samples are excited by a 405 nm continuous wave laser (WITec). The laser was focused through a 100x objective (0.9NA). Emission was collected through the same objective and fed to a fiber coupled spectrometer. A long pass filter(wavelength 488 nm) was used to ensure signal in the long wavelength range and block the reflection of the incoming beam. For calibration. a dark-measurement was done for background subtraction. Figure 45 shows two obtained intensity maps of CdSe, from integrated spectra; dose square and a part of the Fresnel structure. It shows the remaining PL property of the exposed QDs.

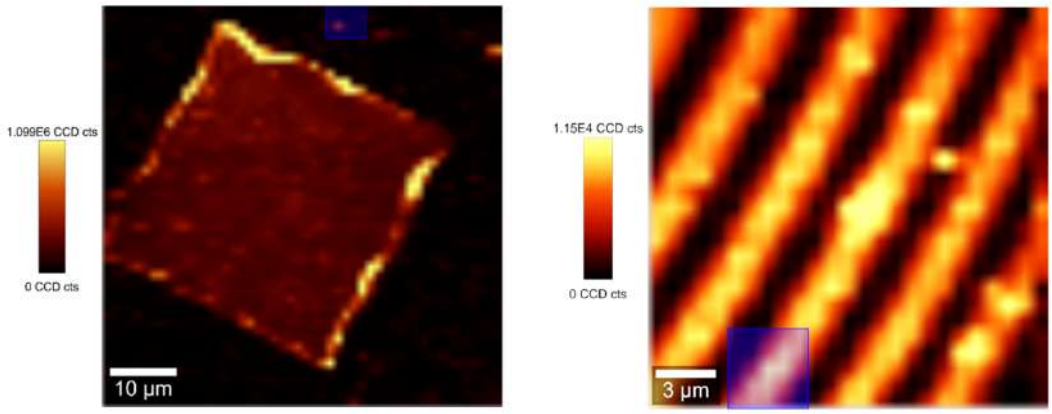

Figure 45: *PL intensity maps of a square dose test and part of the Fresnel pattern.*

Single spectra measurements are conducted of nine different doses, given in figure 46. The PL intensity is plotted as a function of excitation energy. Although the chosen steps of doses are equally separated by $30\mu C/cm^2$, (except between $240\mu C/cm^2$ and $260\mu C/cm^2$), the PL peaks have an unequally separated distribution in the intensity, with two certain thresholds. A higher intensity either means that there more QDs left on the exposed area, or the QDs have kept a higher PLQY compared to the ones that are exposed with a lower dose. A combination of both could also be the explanation.

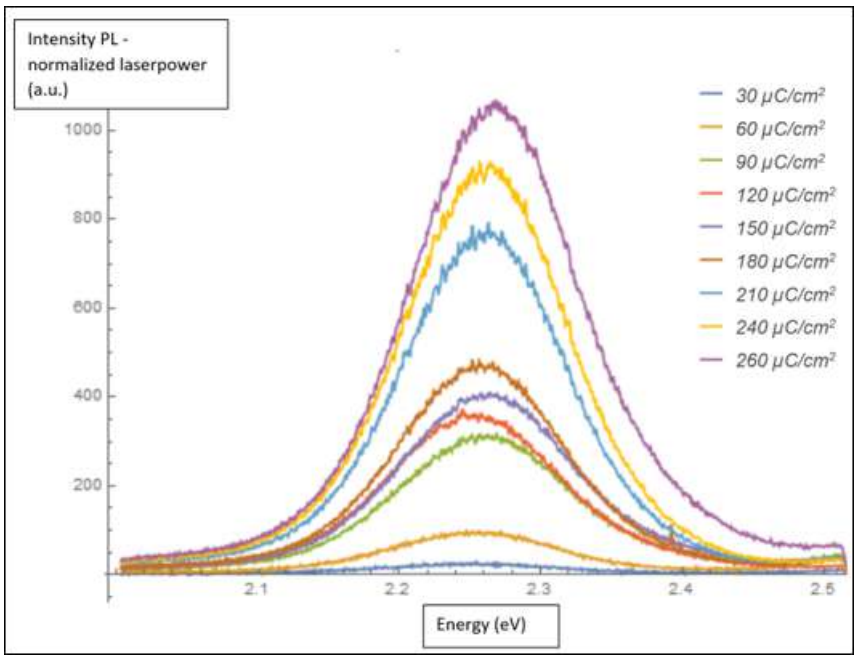

Figure 46: *Single spectra of exposed CdSe with different doses.*

By plotting the peak value against the dose (figure 47), it shows an increasing intensity with increasing electron doses and we see three different linear regions in the graph.

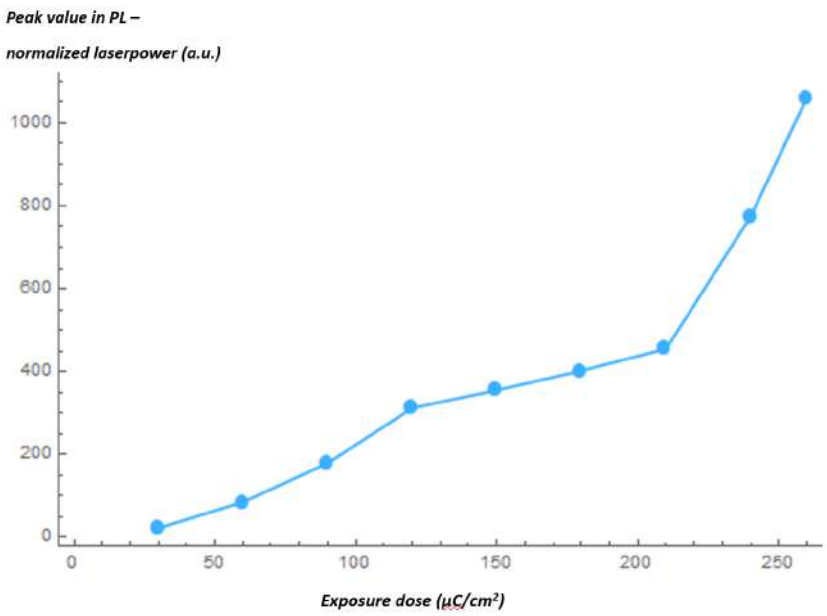

Figure 47: *PL peaks of different doses*

In the range of $90 - 180\mu C/cm^2$ the PL intensity increases with smaller steps. The most important information is that PL remains after exposure.

4.6 Luminescence Characterization: PL decay (Lifetime) - TCSPC

PL decay time (lifetime) is measured and analysed for unexposed and exposed CdSe QDs. The used laser excitation wavelength is 485 nm laser, which is pulsed at 0.5 MHz repetition rate, the laser signal is blocked in the detection path by a long-pass filter(500 nm) combined with a 488 nm notch filter. Unfortunately, the exact dosage was difficult to determine through the systems camera. We have measured different QD areas, with roughly estimated dose ranges. The TCSPC measurement provides a map that contains information on the total amount of photons counted as well as a counted photons over time histogram for every pixel. This allows for comparison of lifetimes between different regions. In our situation, the regions are inhomogeneous, the most consistent way is to measure dose regions with high QD homogeneity, set as *Region of Interest* in the software *SymPhoTime64* and average the data.

As explained in section 2.3, PL decay of QDs consists of multiple decay processes and does not contain a limited number of discrete decay times, but rather a distribution of decay times. Since QDs are surrounded by other QDs, they may effect each other, therefore different decay intensities always occur[52]. Decays are typically analysed in terms of a lifetime distribution, total decay is then the sum of individual decays. The obtained lifetime traces are shown in figure 48. Sample ***A*** is unexposed CdSe, samples ***B,C,D,E,F*** are in the region $100 - 150\mu C/cm^2$, ***G, H*** are in the region $200 - 240\mu C/cm^2$.

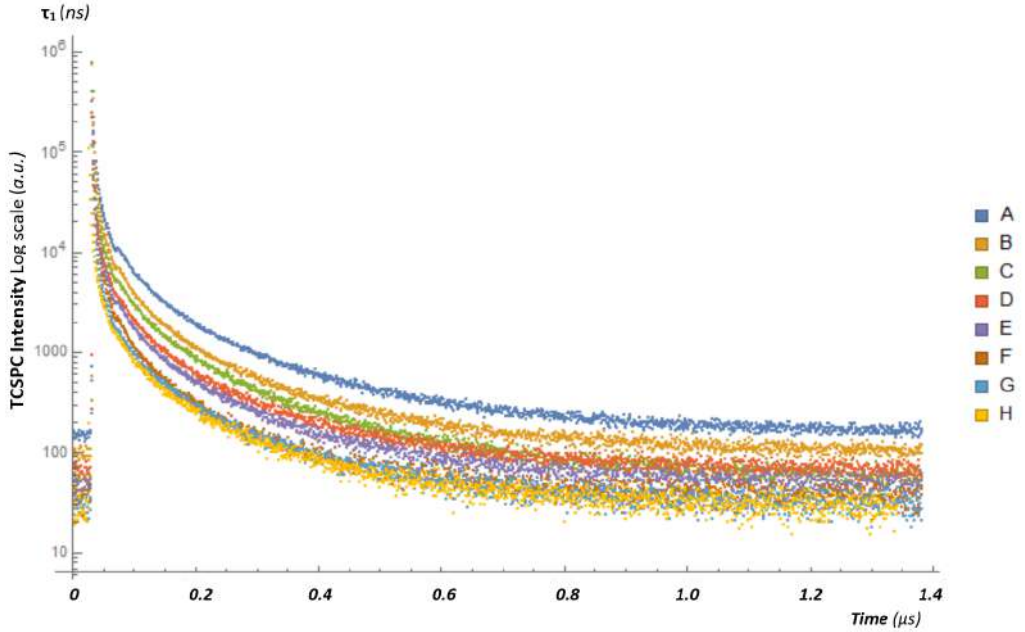

Figure 48: *Fitted PL decay traces of unexposed and different exposed CdSe QD films.*

QDs generally show multi-exponential decay dynamics. Ideally multi-exponential decays should correspond to multiple different sites or excited state populations decaying. Since QD are heterogenous (in size distribution, electron/hole wavefunctions leaking to inorganic/organic shell etc.), multi-exponential decay dynamics is often observed and thus chosen as fiting model. We have chosen the triexponential ($n = 3$) tailfit, as it allows for division of the decay function into three distinct mathematical terms, which can correspond to three distinct physical processes with individual lifetimes and amplitudes. The triexponential function (see 11) provides three different lifetimes along with corresponding amplitudes and a background term:

$$PL(t) = \sum_{n=1}^{3} A_n \cdot e^{\frac{t}{\tau_n}} + PL_{backgr} \tag{11}$$

- PL = photoluminescence lifetime
- t = time
- A_n = Amplitudes
- τ_n = lifetimes or decay times
- PL_{backgr} = background signal

Results show that the amplitude is the highest for the smallest time constant(τ), which means this transition contributes most to the fluorescence of the QDs[52]. Most likely, the smallest value of fitted lifetime refers to radiative decay. Figure 49 shows this fitted component for the doses, including error-bars.

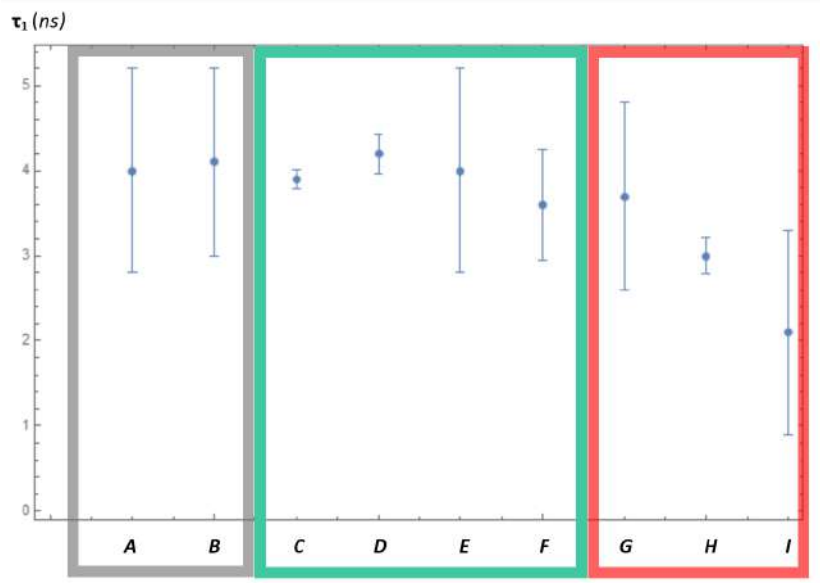

Figure 49: *Shortest lifetime τ_1 component after fitting, of unexposed and exposed CdSe QD films. In the grey frame are unexposed samples, in green medium exposed (*$100-150\mu C/cm^2$*), and in red* $200-240\mu C/cm^2$

We do not assign specific meaning to the other two obtained lifetimes with the 3-exponential fit, it is difficult to distinguish and quantify, relating to non-radiative decays. Some literature assigns the longest decay time component to non-radiative decay such as to band edge and the deep trap recombinations[52]. But evidence is yet to be investigated. Figure 50 shows the longest lifetime components of all samples, including error bars, we do observe the same patterns as with τ_1.

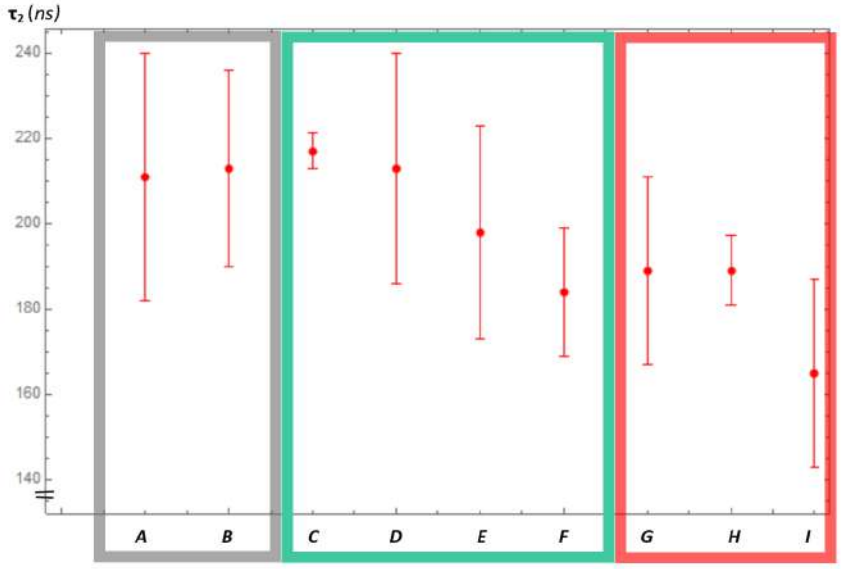

Figure 50: *Longest lifetime τ_2 component after fitting, of unexposed and exposed CdSe QD films. In the grey frame are unexposed samples, in green medium exposed ($100-150\mu C/cm^2$), and in red $200-240\mu C/cm^2$*

A small decrease in radiative decay occurs, but rates of emission are relatively constant upon exposure. We conclude that exposure does not affect the lifetimes of CdSe significantly.

4.7 Future work

For future work, many proves are still needed for the cross-linking mechanism, especially the cross-link location in the ligands. The presence of double bonds can be identified for before and after exposure, also to what extend. Different ligands can be applied to prove the difference in double bonds. Furthermore, to gain more information about the exact mechanism that occurs during exposure, analyses such as lifetime and PLQY measurements can be conducted for before and after exposed QDs. For investigation into detailed difference in PL stability, emission rate, and quantifying the loss in PLQY with the exposure dose. Improvements on the experimental method are also needed, such as substrate attachment, optimal development ratio of solvents, type of development solvent.

The future of QDs as resist lies mainly in nanophotonic application. The ultimate resolution is to reach the scale of a few QDs, as direct-write lithography operates through the cross-linking of surface ligands between adjacent QDs, the final achievable resolution cannot be as small as a single QD, but this could be realized by cross-linking the single QD to an interlayer that also has organic molecules. In this case, the interaction between the interlayer and the QD could only become specific under irradiation. To achieve single QD arrays with this method, it has to be ensured that upon irradiation, only QDs and interlayer are cross-linked and not QDs with QDs. This is quite difficult to achieve.

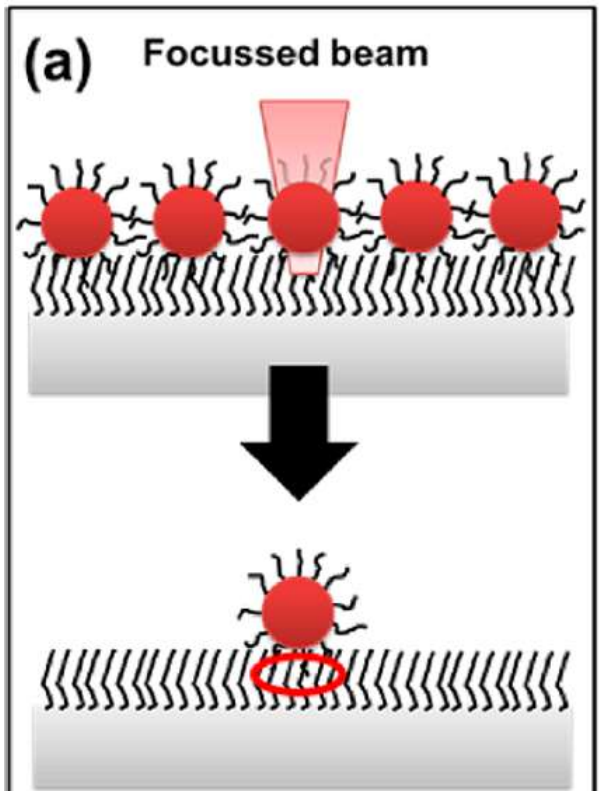

Figure 51: *Schematic representation of possible single-NC patterning through specific cross-linking of surface ligands with functionalized substrate.*

5 Conclusion

PbS and CdSe QDs were synthesized through hot-injection method, their diameters are approximately 3 nm and 5 nm respectively. It is possible to create nanostructures in both PbS and CdSe QD films with direct e-beam lithography. Before the exposure, the QDs are dispersible in hydrophobic solutions such as toluene, octane and hexane. During exposure to electrons, the ligand structures become altered by kinetic energy of the electrons. It appears from CASINO simulations that most of the electrons go through the substrate, only a small fraction enter the QDs as secondary electrons, these electrons deposit kinetic energy leading to cross-linking between the ligands. The optimal dose range is $80 - 200\mu C/cm^2$ for both CdSe and PbS. For the attachment of PbS to the substrate, MUDA is a suitable linker molecule.

Results show that after the substrate development in toluene-IPA, the exposed parts of the QD film can no longer be dispersed and remain on the substrate, while the unexposed parts QDs still disperse and can be rinsed off of the substrate. Resolution limit of patterning PbS and CdSe are realized down to 20 nm, which is small compared to photolithography. The dose threshold was quantified for the different QD systems. The remaining PL properties show an increasing intensity with increasing exposure dose. Furthermore, exposed QD lines become stretched out, which indicates cross-link between the ligands, and their PL and lifetime of radiative decay remain. More experiments are underway to find out the origin of PL quenching at different e-beam exposure dosages.

References

[1] AN Broers, ACF Hoole, and JM Ryan. Electron beam lithography—resolution limits. *Microelectronic Engineering*, 32(1-4):131–142, 1996.

[2] Greg Parker. Encyclopedia of materials: science and technology. 2001.

[3] DM Tennant and AR Bleier. Electron beam lithography of nanostructures. *Handbook of Nanofabrication (Elsevier, Amsterdam 2010) Chap*, 4:121–148, 2010.

[4] Moshe Preil. Factors that determine the optimum dose for sub-20nm resist systems: Duv, euv, and e-beam options. In *Advances in Resist Materials and Processing Technology XXIX*, volume 8325, page 832503. International Society for Optics and Photonics, 2012.

[5] Markos Trikeriotis, Woo Jin Bae, Evan Schwartz, Marie Krysak, Neal Lafferty, Peng Xie, Bruce Smith, Paul A Zimmerman, Christopher K Ober, and Emmanuel P Giannelis. Development of an inorganic photoresist for duv, euv, and electron beam imaging. In *Advances in Resist Materials and Processing Technology XXVII*, volume 7639, page 76390E. International Society for Optics and Photonics, 2010.

[6] Vikas Nandwana, Chandramouleeswaran Subramani, Yi-Cheun Yeh, Boqian Yang, Stefan Dickert, Michael D Barnes, Mark T Tuominen, and Vincent M Rotello. Direct patterning of quantum dot nanostructures via electron beam lithography. *Journal of Materials Chemistry*, 21(42):16859–16862, 2011.

[7] Dmitri V Talapin, Jong-Soo Lee, Maksym V Kovalenko, and Elena V Shevchenko. Prospects of colloidal nanocrystals for electronic and optoelectronic applications. *Chemical reviews*, 110(1):389–458, 2009.

[8] Yasuhiro Shirasaki, Geoffrey J Supran, Moungi G Bawendi, and Vladimir Bulović. Emergence of colloidal quantum-dot light-emitting technologies. *Nature photonics*, 7(1):13, 2013.

[9] Harinder Arya, Zeenia Kaul, Renu Wadhwa, Kazunari Taira, Takashi Hirano, and Sunil C Kaul. Quantum dots in bio-imaging: revolution by the small. *Biochemical and biophysical research communications*, 329(4):1173–1177, 2005.

[10] Raghavendra Palankar, Nikolay Medvedev, Alena Rong, and Mihaela Delcea. Fabrication of quantum dot microarrays using electron beam lithography for applications in analyte sensing and cellular dynamics. *ACS nano*, 7(5):4617–4628, 2013.

[11] KAUL Zeenia, Tomoko Yaguchi, C KAUL Sunil, Takashi Hirano, Renu Wadhwa, and Kazunari Taira. Mortalin imaging in normal and cancer cells with quantum dot immuno-conjugates. *Cell research*, 13(6):503, 2003.

[12] Francisco Palazon, Mirko Prato, and Liberato Manna. Writing on nanocrystals: patterning colloidal inorganic nanocrystal films through irradiation-induced chemical transformations of surface ligands. *Journal of the American Chemical Society*, 139(38):13250–13259, 2017.

[13] Siqi Ma, Celal Con, Mustafa Yavuz, and Bo Cui. Polystyrene negative resist for high-resolution electron beam lithography. *Nanoscale research letters*, 6(1):446, 2011.

[14] Martin Feldman. *Nanolithography: the art of fabricating nanoelectronic and nanophotonic devices and systems*. Woodhead publishing, 2014.

[15] The University of Sheffield. Electron beam lithography. `https://www.sheffield.ac.uk/ebl/patterning`, 2011. [Online; accessed 26-November-2019].

[16] Yu-Ming He, Genevieve Clark, John R Schaibley, Yu He, Ming-Cheng Chen, Yu-Jia Wei, Xing Ding, Qiang Zhang, Wang Yao, Xiaodong Xu, et al. Single quantum emitters in monolayer semiconductors. *Nature nanotechnology*, 10(6):497, 2015.

[17] Charles Kittel, Paul McEuen, and Paul McEuen. *Introduction to solid state physics*, volume 8. Wiley New York, 1996.

[18] Chaudhery Mustansar Hussain. *Handbook of Nanomaterials for Industrial Applications*. Elsevier, 2018.

[19] Lukas Novotny and Bert Hecht. *Principles of nano-optics*. Cambridge university press, 2012.

[20] Hilmi Volkan Demir and Sergey V Gaponenko. *Applied nanophotonics*. Cambridge University Press, 2018.

[21] Marc A Kastner. Artificial atoms. *Physics today*, 46:24–24, 1993.

[22] David Andrews, Gregory Scholes, and Gary Wiederrecht. *Comprehensive nanoscience and technology*. Academic Press, 2010.

[23] Danylo Zherebetskyy, Marcus Scheele, Yingjie Zhang, Noah Bronstein, Christopher Thompson, David Britt, Miquel Salmeron, Paul Alivisatos, and Lin-Wang Wang. Hydroxylation of the surface of pbs nanocrystals passivated with oleic acid. *Science*, 344(6190):1380–1384, 2014.

[24] Manu Mitra. Multiple quantum dot tunneling in a semiconductor and its wave function and probability density. 2018.

[25] Jie Zhou, Yun Liu, Jian Tang, and Weihua Tang. Surface ligands engineering of semiconductor quantum dots for chemosensory and biological applications. *Materials Today*, 20(7):360–376, 2017.

[26] Talgat M Inerbaev, Artëm E Masunov, Saiful I Khondaker, Alexandra Dobrinescu, Andrei-Valentin Plamadă, and Yoshiyuki Kawazoe. Quantum chemistry of quantum dots: Effects of ligands and oxidation. *The Journal of chemical physics*, 131(4):044106, 2009.

[27] Eloisa Berbel Manaia. *Zinc oxide (ZnO) based quantum dots for bioimaging applications of lipid nanocarriers*. PhD thesis, 2016.

[28] Graham H Carey, Ahmed L Abdelhady, Zhijun Ning, Susanna M Thon, Osman M Bakr, and Edward H Sargent. Colloidal quantum dot solar cells. *Chemical reviews*, 115(23):12732–12763, 2015.

[29] Jing Chen, JL Song, XW Sun, WQ Deng, CY Jiang, W Lei, JH Huang, and RS Liu. An oleic acid-capped cdse quantum-dot sensitized solar cell. *Applied physics letters*, 94(15):153115, 2009.

[30] Kurt Scheerschmidt and Peter Werner. Characterization of structure and composition of quantum dots by transmission electron microscopy. In *Nano-Optoelectronics*, pages 67–98. Springer, 2002.

[31] Michael Wahl. Time-correlated single photon counting. *Technical Note*, pages 1–14, 2014.

[32] Marat Lutfullin, Lutfan Sinatra, and Osman M Bakr. Quantum dots for electronics and energy applications.

[33] Wolfgang Becker. *Advanced time-correlated single photon counting techniques*, volume 81. Springer Science & Business Media, 2005.

[34] The Engineers Post. Electron-beam machining (ebm): Working principle, advantage, limitation and design. `https://www.theengineerspost.com/electron-beam-machining/`, 2012. [Online; accessed 26-November-2019].

[35] Vitor R Manfrinato, Jianguo Wen, Lihua Zhang, Yujia Yang, Richard G Hobbs, Bowen Baker, Dong Su, Dmitri Zakharov, Nestor J Zaluzec, Dean J Miller, et al. Determining the resolution limits of electron-beam lithography: direct measurement of the point-spread function. *Nano letters*, 14(8):4406–4412, 2014.

[36] Richard A Lawson and Alex PG Robinson. Overview of materials and processes for lithography. In *Frontiers of Nanoscience*, volume 11, pages 1–90. Elsevier, 2016.

[37] Jing Jiang, Danilo De Simone, and Geert Vandenberghe. Difference in euv photoresist design towards reduction of lwr and lcdu. In *Advances in Patterning Materials and Processes XXXIV*, volume 10146, page 101460A. International Society for Optics and Photonics, 2017.

[38] Kannan Seshadri, Karl Froyd, Atul N Parikh, David L Allara, Michael J Lercel, and Harold G Craighead. Electron-beam-induced damage in self-assembled monolayers. *The Journal of Physical Chemistry*, 100(39):15900–15909, 1996.

[39] Francisco Palazon, Quinten A Akkerman, Mirko Prato, and Liberato Manna. X-ray lithography on perovskite nanocrystals films: from patterning with anion-exchange reactions to enhanced stability in air and water. *ACS nano*, 10(1):1224–1230, 2015.

[40] Jose L Plaza, Yu Chen, Susanne Jacke, and Richard E Palmer. Nanoparticle arrays patterned by electron-beam writing: structure, composition, and electrical properties. *Langmuir*, 21(4):1556–1559, 2005.

[41] J Lohau, S Friedrichowski, G Dumpich, EF Wassermann, M Winter, and MT Reetz. Electron-beam lithography with metal colloids: Direct writing of metallic nanostructures. *Journal of Vacuum Science & Technology B: Microelectronics and Nanometer Structures Processing, Measurement, and Phenomena*, 16(1):77–79, 1998.

[42] Xiaozhou Ye and Limin Qi. Two-dimensionally patterned nanostructures based on monolayer colloidal crystals: Controllable fabrication, assembly, and applications. *Nano Today*, 6(6):608–631, 2011.

[43] Harvard. Schlieren. `https://sciencedemonstrations.fas.harvard.edu/presentations/schlieren-optics`, 2019. [Online; accessed 02-December-2019].

[44] WJ Daughton and FL Givens. An investigation of the thickness variation of spun-on thin films commonly associated with the semiconductor industry. *Journal of The Electrochemical Society*, 129(1):173–179, 1982.

[45] Dominique Drouin, Pierre Hovington, and Raynald Gauvin. Casino: A new monte carlo code in c language for electron beam interactions—part ii: Tabulated values of the mott cross section. *Scanning*, 19(1):20–28, 1997.

[46] Pierre Hovington, Dominique Drouin, and Raynald Gauvin. Casino: A new monte carlo code in c language for electron beam interaction—part i: Description of the program. *Scanning*, 19(1):1–14, 1997.

[47] John J Biafore and Mark D Smith. Application of stochastic modeling to resist optimization problems. In *Advances in Resist Materials and Processing Technology XXIX*, volume 8325, page 83250H. International Society for Optics and Photonics, 2012.

[48] Aidan AE Fisher, Mark A Osborne, Iain J Day, and Guillermo Lucena Alcalde. Measurement of ligand coverage on cadmium selenide nanocrystals and its influence on dielectric dependent photoluminescence intermittency. *Communications Chemistry*, 2(1):63, 2019.

[49] Lei Jiang, Songyan Li, Jiqian Wang, Limin Yang, Qian Sun, and Zhaomin Li. Surface wettability of oxygen plasma treated porous silicon. *Journal of Nanomaterials*, 2014:8, 2014.

[50] Daniel Bonn, Jens Eggers, Joseph Indekeu, Jacques Meunier, and Etienne Rolley. Wetting and spreading. *Reviews of modern physics*, 81(2):739, 2009.

[51] Yi Pan, Yue Ru Li, Yu Zhao, and Daniel L Akins. Synthesis and characterization of quantum dots: a case study using pbs. *Journal of Chemical Education*, 92(11):1860–1865, 2015.

[52] Gurvir Kaur, Harmandeep Kaur, and SK Tripathi. Fluorescence relaxation dynamics of cdse and cdse/cds core/shell quantum dots. In *AIP Conference Proceedings*, volume 1591, pages 420–422. American Institute of Physics, 2014.